AMERICAN UNIVERSITY OF BEIRUT

# A METATHESIS MODEL FOR ESTER HYDROGEATION BY A RUTHENIUM OCTAHEDRAL COMPLEX USING DFT CALCULATIONS

by
HASSAN MOHAMMAD HARB

A thesis
submitted in partial fulfillment of the requirements
for the degree of Master of Sciences
to the Department of Chemistry of
the Faculty of Arts and Sciences
at the American University of Beirut

Beirut, Lebanon
June 2015

AMERICAN UNIVERSITY OF BEIRUT

# A METATHESIS MODEL FOR ESTER HYDROGEATION BY A RUTHENIUM OCTAHEDRAL COMPLEX USING DFT CALCULATIONS

by

HASSAN MOHAMAD HARB

Approved by:

Dr. Faraj Hasanayn, PhD. — Advisor
Chemistry Department

Dr. Mazen Al-Ghoul, PhD — Member of Committee
Chemistry Department

Dr. Houssam El-Rassy, PhD — Member of Committee
Chemistry Department

Date of thesis defense: June 16, 2015

# AMERICAN UNIVERSITY OF BEIRUT

# THESIS, DISSERTATION, PROJECT RELEASE FORM

Student Name:

| Harb | Hassan | Mohammad |
|---|---|---|
| Last | First | Middle |

◉ Master's Thesis ○ Master's Project ○ Doctoral Dissertation

☐ I authorize the American University of Beirut to: (a) reproduce hard or electronic copies of my thesis, dissertation, or project; (b) include such copies in the archives and digital repositories of the University; and (c) make freely available such copies to third parties for research or educational purposes.

☑ I authorize the American University of Beirut, **three years after the date of submitting my thesis, dissertation, or project,** to: (a) reproduce hard or electronic copies of it; (b) include such copies in the archives and digital repositories of the University; and (c) make freely available such copies to third parties for research or educational purposes.

| [signature] | 22-9-2015 |
|---|---|
| Signature | Date |

# ACKNOWLEDGMENTS

First and foremost, I would like to express my genuine thankfulness to my adviser Dr Faraj Hasanayn and I feel being indebted to him for having one special mentor for the past years and for knowing that regardless of all the barriers we faced, his guidance and encouragement just had me pushing forward with my work.

I also would show my sincere gratitude to Dr Mazen Ghoul and Dr Houssam El Rassy, my thesis committee for helping me throughout the whole journey up until the very end.

I would also like to show my gratefulness to the entire faculty, staff members, and the current and past graduate students in the Chemistry Department at AUB for their continuous support in the past years, special thanks for Lubna, Zeinab, Mazhar, Antranik, Maya, Sandrine, Christina, Julie, Ahmad, Dani, Ali, Elsy, Rasha, Samir, Nayri, Hala, Razan, Mira, and Sara.

Special thanks for the University Research Board, AUB IT department, and the High Performance Computing (HPC) facility at AUB and the IT Research Computing group in Texas A&M University at Qatar for providing me with the suitable computational resources.

Also, I would express deep gratitude to the Chemistry professors at LAU for helping me throughout the first step in my journey, namely Dr Samira Korfali, Dr Ahmad Kabbani, Dr Ahmad Houri and Dr Jomana Elaridi.

I would also express my deep appreciation to my childhood friends Ali, Zaher, Ahmad, Mahmoud, Farah, Sireen, Diala, Jinane, Sara, Jad and all the others. Also I would show my thankfulness to all the friends in AUB Secular Club, Red Oak club and Alternative Student Movement, who showed me that scientific achievements are nothing but a part of our struggle for a better society. Sincere appreciation goes to Luna, Ali F., Ali Z., Zakaria, Yara, Sara, Lynn, Zeinab, Ahmad T., Ahmad E., Rami, Mohamad, Walid, Elsa, Hala, Jinan, Ellen, Nadine, Karim, Azza, Ibrahim, Yasmina, Shadi, and Abbas.

I would be honored to thank my father and my mother, and to my siblings Dana, Yara, and Ribal, for bearing with me during all the stressful times, and to all the friends and family members who accompanied me during this journey.

# AN ABSTRACT OF THE THESIS OF

Hassan Mohammad Harb for Master of Science
Major: Chemistry

Title: A METATHESIS MODEL FOR ESTER HYDROGEATION BY A RUTHENIUM OCTAHEDRAL COMPLEX USING DFT CALCULATIONS

Electronic structure DFT method had been used to investigate the mechanism of ester hydrogenation by a known octahedral ruthenium hydride catalyst having a PNN pincer type ligand. Our results identified a direct low-energy reaction path connecting the ester and the octahedral ruthenium hydride with an octahedral ruthenium alkoxide and an aldehyde. This path represents a novel ion-pair metathesis mode in which a hydride and an alkoxide are exchanged between a metal and an acyl group in an outer sphere mode. A related path is computed for the reaction of a carboxamide. The given reaction path provides a new perspective to understanding the mechanism of the given catalyst that is radically different from the generally accepted metal-ligand cooperation mechanism invoking a formation and reaction of a hemiacetal. The calculations are also used to identify new complexes that may be used to support the proposed mechanism experimentally.

# CONTENTS

To my heroic father and my caring mother, and to my lovely siblings Dana, Yara, and Ribal.

To the late Hassan Ismail who was one big loss for me during this journey, and to every person that is fighting against injustice all over the world.

To the children of Palestine and Syria who definitely deserve a better life away from all the unfairness.

To Zeinab, a very special person who showed me that life is not worth living if it were not full of challenges and that we should always strive for what we dream for.

# CHAPTER I

# INTRODUCTION

## A. Green Chemistry

The concept of greening chemistry is a relatively new idea in the business and regulatory communities that evolved from pollution prevention initiatives.[1] The concept of Green Chemistry has had this large impact due to the fact that it goes beyond the research laboratory in isolation and has touched industry, education, environment, and the general public.[2] In our efforts to improve crop protection, commercial products, and medicines, we also caused unintended harm to our planet and humans. For this fact, the world has been deviating away from classical chemical processes to ones that would rather cause less harm to the environment. One of the major goals of catalysis today is the design of environmentally benign, atom-economical processes, to replace traditional, waste forming reactions, including some of the most fundamental synthetic methods.[3] In addition, due to the resource depletion and environmental concerns, chemists and chemical industries have been working to discover environmentally benign synthetic methods and sustainable catalytic reactions that avoid toxic reagents and waste productions.

The most important aspect of Green Chemistry is the concept of design. Design is a statement of human intention and one cannot do design by accident. It includes novelty, planning and systematic conception. The Twelve Principles of Green Chemistry are “design rules” to help chemists achieve the intentional goal of

sustainability. Green Chemistry is characterized by careful planning of chemical synthesis and molecular design to reduce adverse consequences. [2]

### B. Methods for Ester Hydrogenation

Ester hydrogenation has been performed using stoichiometric amounts of the ester and $LiAlH_4$. This reducing agent is widely used in organic synthesis and it can hydrogenate all carboxylic acids, carbonic acids and their respective derivatives.[4] However, the main drawback of this reaction is the production of hazardous metal oxides and metal hydrides that pose serious environmental concerns especially on the aquatic life. [5]

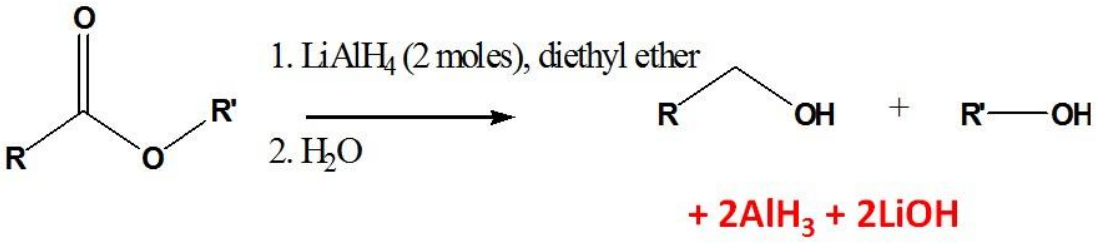


In addition, this reagent is not ideal from the perspective of cost, safety and simplicity of work-up procedures. $LiAlH_4$ is extremely flammable and highly reactive towards water, this could possess hazardous threats to the experimental setup. Also, $LiAlH_4$ is prepared from the reaction of LiH and $AlCl_3$ followed by filtration to remove LiCl byproducts. [6]

$$4\ LiH + AlCl_3 \rightarrow LiAlH_4 + 3\ LiCl$$

The use of hydrogen gas for ester reduction would obviously provide an alternative to $LiAlH_4$ reduction that will be atom economical and won't generate any waste.[7]

Considering studying esterification and hydrogention reactions, which are fundamental and significant chemical reactions in synthesis of organic compounds, various methodologies have been established, developed and are being currently used in chemical synthesis.[8, 9] Classically, esterification has been performed using an acid catalyzed reaction that uses stiochiometric ratios of a carboxylic acid and an alcohol and that produces esters and water.[10]

$$RCOOH + R'OH \rightarrow RCOOR' + H_2O$$

Alternative methods have been investigated and esters have been synthesized without the need of a carboxylic acid or any of its derivatives. An attractive approach was developed which focused on the dehydrogenative coupling of alcohols and amines into esters and carboxamides, such reactions would result in the evolution of Hydrogen gas as an only product.

In an attempt to green this chemistry, in recent years new classes of homogeneous catalysts were developed to conduct the hydrogenation reaction with $H_2$. Reactions mediated by the transition metal complexes have been applied widely both in synthesis and as catalysts to mediate the hydrogenation of esters and carboxamides to alcohols and amines[3]. These reactions can be facilitated by the cooperation of the non innocent ligands and the metal center by undergoing reversible chemical and structural changes. [7, 11, 12]

Milstein and coworkers have designed a new class of transition metal complexes where the ligand is a type of non innocent pincer ligand that supports metal-

ligand cooperation mechanism which appears to involve an aromatization-dearomatization process of the pyridine or acridine-based PNP and PNN “pincer” ligands. These complexes were reported to lead to the unusual X-H (X=H, C, O, N, and B) activation reactions and to environmentally benign catalysis involving dehydrogenation and hydrogenation reactions. Several reviews by Milstein and coworkers have appeared that give an overview of the experimental studies of these chemical reactions mediated by their designed complexes.[8, 13-15]

### C. Pincer Ligands

Pincer ligands are one class of chelating agents that bind tightly to three adjacent coplanar sites, a transition metal in a meridional configuration.[16] Such ligands are categorized by the nature of donor atoms along the ligand scaffold and they are usually referred to as DXD, having D indicating the flanking donors and X being the central anchoring donor. [17]

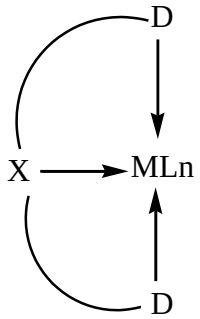


**Figure 1.1:** An illustration of the general structure of a tridentate pincer ligand

Significantly, the realization that pincer ligands offer both a unique, highly protective environment for the coordinated metal center and opportunities to fine-tune the steric and electronic properties of the metal atom has generated extensive research

into the use of these complexes as catalysts.[18] The research on metal-ligand complexes where the latter are phosphine-based pincer complexes has been an influence on numerous researches.[19, 20] The first metal complexes having pincer ligands have the PCP structure, indicating that the ligand consists of two phosphine arms interconnected by a hydrocarbon chain that could be either aromatic or aliphatic.[19] The phosphine arms can also accommodate alkyl or aryl groups, the general structures of such pincer ligands are given below where R could be either an alkyl or an aryl group:

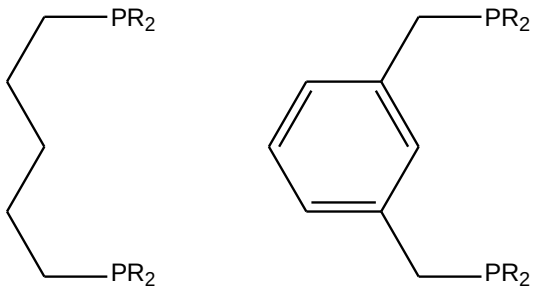


Metal pincer complexes are typically robust structures with high thermal stability and many researchers are currently investigating pincer complexes for various applications ranging from homogeneous catalysis to the development of chemical sensors and switches.[16]

A key feature about pincer based metal complexes is that such metals provide a special balance between the stability of the complex and its reactivity. Both aspects, can be optimized by modifying the pincer or part of it, or in other reported cases, modifying the metal center. Such modifications would eventually lead to an enhancement in the metal complex reactivity in addition to increase in selectivity of the complex and providing a new aspect for fundamental insights for particular reaction systems.[19, 21]

Catalyst designs that depicted Ruthenium (II) as its metal center were reported by Van Koten et. al. Their pincer ligand catalyst had NCN and PCP as the ligands and were reported to catalyze the hydrogenation of ketones to their respective alcohols, such reactions could proceed only in presence of a strong base, e.g. KOH. The significance of such reactions were that they were of great attention since they were one of the leading pincer complexes which showed practical simplicity and potential use at ambient pressure; such conditions are critical for the search for optimized systems for essential chemical reactions.[22, 23]

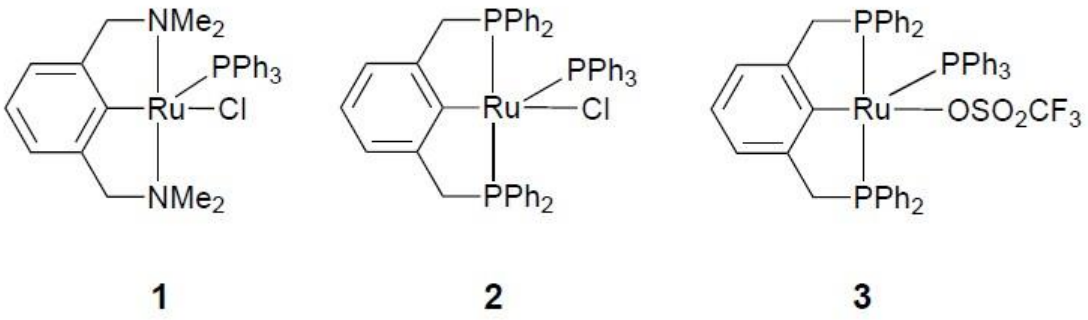


**Figure 1.2:** Three different Ru (II) complexes having NCN (1) and PCP (2 and 3) pincer ligands

### D. Bond Activation by Metal-Ligand Cooperation

PNN Pincer ligands such as ((2-(di-tert-butyl phosphinomethyl)-6-diethyl amino methyl) pyridine) coordinate with the metal via three sites: phosphine arm, pyridine ring and amine arm. These ligands are electron-rich groups and therefore are also classified as electron donating groups so they would have the ability to stabilize the

unsaturated metal center. The planar geometry of the pyridine ring would provide a suitable space for possible metal-substrate interaction.[11, 12, 24]

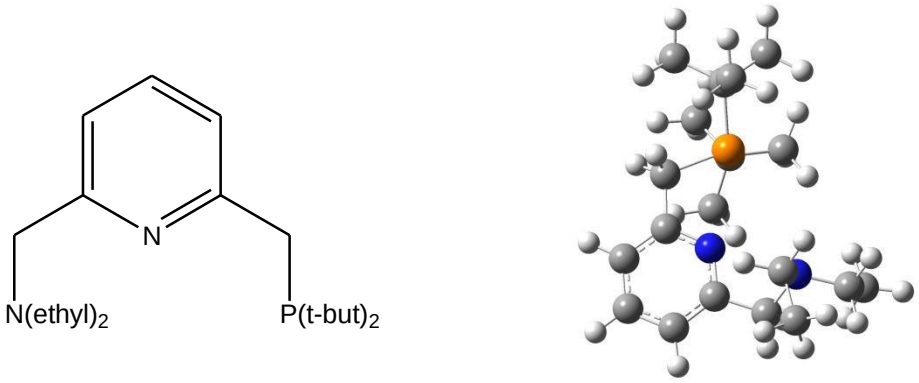


**Figure 1.3:** An Example of a PNN Pincer ligand in 2-D (left) and 3-D structure optimized using Gaussian 09 software and visualized using GaussView

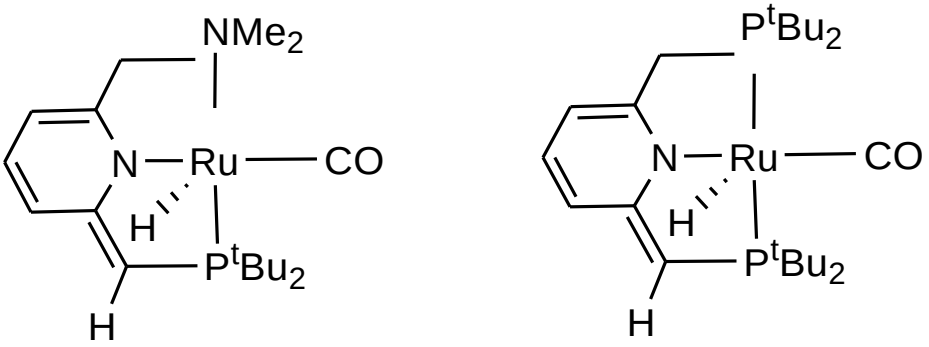


**Figure 1.4:** Milstein's Square pyramidal Ruthenium PNN pincer catalyst (left) and PNP catalyst (right)

Milstein's catalyst [Ru(PNN)(CO)(H)] is a square pyramidal metal complex that is a prototype of pincer ligated complexes. Such complexes are known to add $H_2$ reversibly, with a heterolytic bond cleavage of the hydrogen molecule, via a metal-ligand cooperation mechanism in which the proton adds to the methylene linker neighboring the phosphine arm of the ligand and the hydride adds to the metal to form

octahedral Ruthenium complexes in which the hydrides are trans with respect to each other. [11, 12]

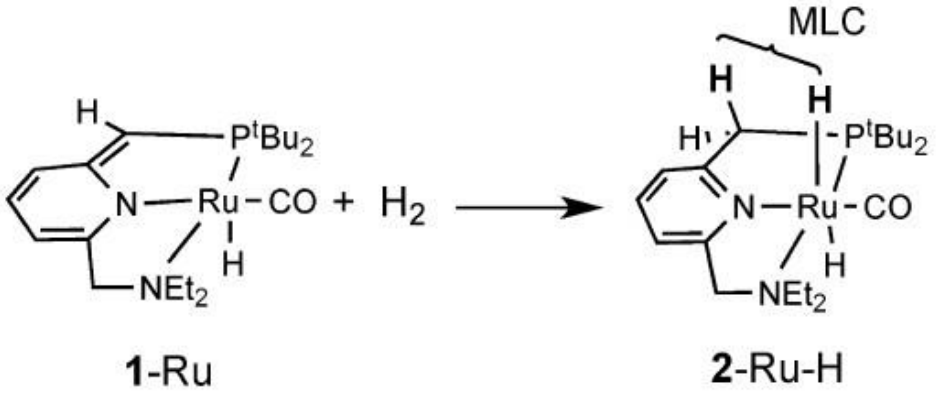


**Figure 1.5:** $H_2$ addition to square pyramidal Ruthenium PNN catalyst via Metal-Ligand Cooperation

In addition to $H_2$ addition, 1-Ru is reported to perform various other additions to the initially square pyramidal complex. Of these additions, we report here relevant ones to our study, such reactions include the addition of R-OH,and R-$NH_2$ additions to the 1-Ru square pyramidal complex:

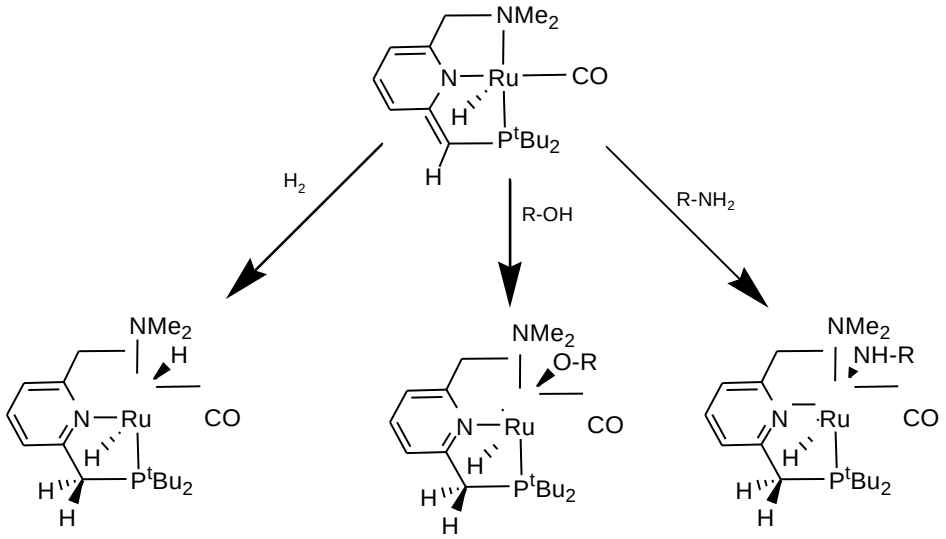


**Figure 1.6:** $H_2$, R—OH and R—$NH_2$ additions to the square pyramidal complex

Milstein's reported study indicates an efficient and selective class of catalysts that are capable of transforming primary alcohols into esters with an evolution of $H_2$ gas, the reactions are also found to be done at relatively mild and neutral conditions, unlike the previously reported chemical synthesis where the reaction either should be acid or base catalyzed or a stiochiometric amount of a reducing agent is needed.[3, 12]

### E. Catalysis by PNN complexes

Milstein's group reported that the square pyramidal Ruthenium complex (1-Ru), in presence of $H_2$ gas, catalyzes the hydrogenation of esters and carboxamides into alcohols and amines according to the following equation:

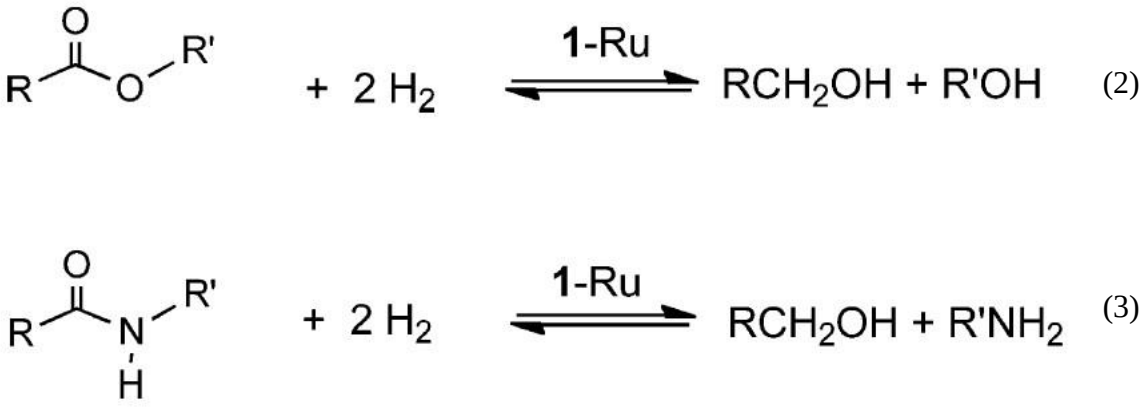


**Figure 1.7:** Equations (2) and (3): Hydrogenation of Esters and carboxamides into alcohols and amines respectively, catalyzed by 1-Ru under $H_2$ atmosphere

Such a system developed by Milstein and co. which is based on the formation of ester and carboxamide bonds under neutral conditions involves a dehydrogenative coupling of alcohols and amines using 1-Ru as the corresponding catalyst. Remarkably Milstein's group was able to adapt the reverse of equations (2) and (3) to promote the production of esters and carboxamides by coupling of alcohols and amines under reflux

and using the same square pyramidal complex with a clean process that would only produce $H_2$ gas as a byproduct.[8]

In addition, the dehydrogenative coupling of alcohols by 1-Ru catalyst catalyzes trans esterification and amidation of esters and amines respectively. Such reactions are also of great importance in chemical synthesis and the mentioned chemical processes occur as well in an eco-friendly manner and is atom economical. [25, 26]

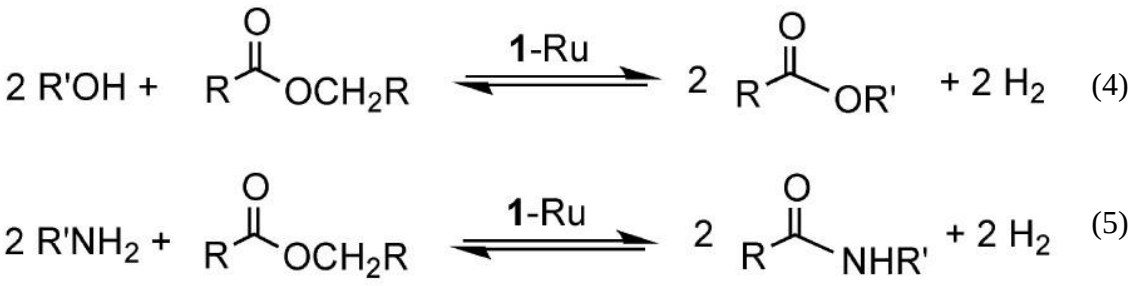


**Figure 1.8:** Equations (4) and (5) transesterification processes of esters with alcohols and amines catalyzed by 1-Ru

### F. Mechanistic studies for the potential energy surface for the dehydrogenative coupling of alcohols and amines into esters and carboxamides

An understanding of the mechanisms can help researchers to improve the current reactions and design new reactions. Thus the mechanism of catalysis by 1-Ru has been studied theoretically. Studies focused on an important role for the ligand in hydrogenation, where the reaction occurs via metal-ligand cooperative mechanism that in turn includes reversible aromatization-dearomatization of ligands.[9]

## 1. Metal-Ligand Cooperation Mechanism (MLC)

Initially, the mechanism was proposed to follow a Metal-Ligand Cooperative mechanism that imposes 1-Ru and hemiacetals as intermediates for ester hydrogenation, and 1-Ru and hemiaminals for carboxamide hydrogenation has been known to be a generally accepted mechanism.[27, 28]

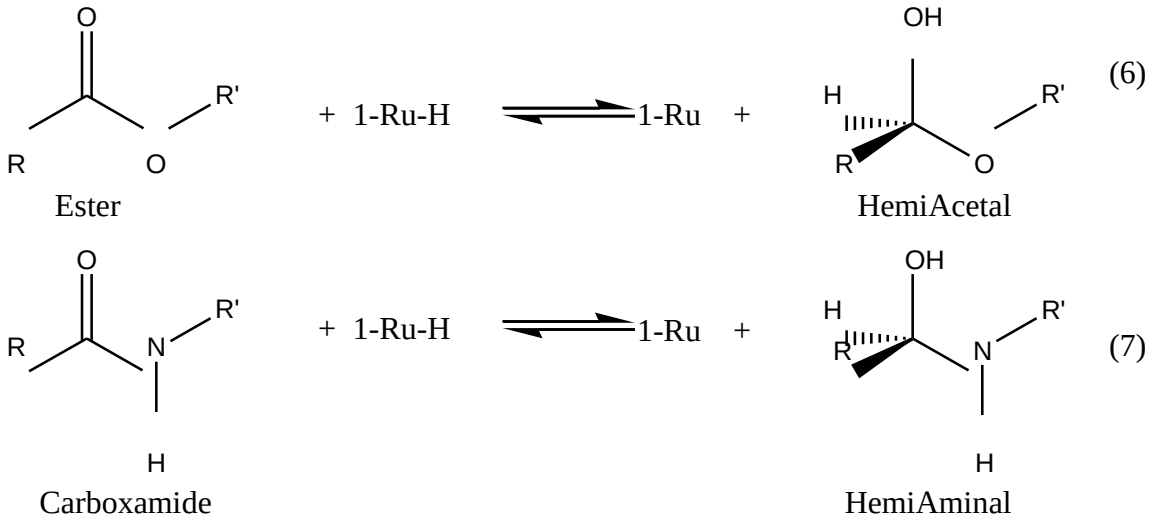


**Figure 1.9:** Equations (6) and (7) showing the formation of the hemiacetals and hemiaminals by the reaction of esters and carboxamides with 1-Ru-H respectively

The given MLC reactions are related to the bifunctional reactions invoked by Noyori to account for ketone hydrogenation by octahedral and piano stool ruthenium-amino hydride catalysts (HRu-NH) where the amino group serves as the proton donor. Noyori proposed bifunctional hydrogenation to take place in an outer-sphere mode without prior coordination of the ketone to the metal.[29, 30]

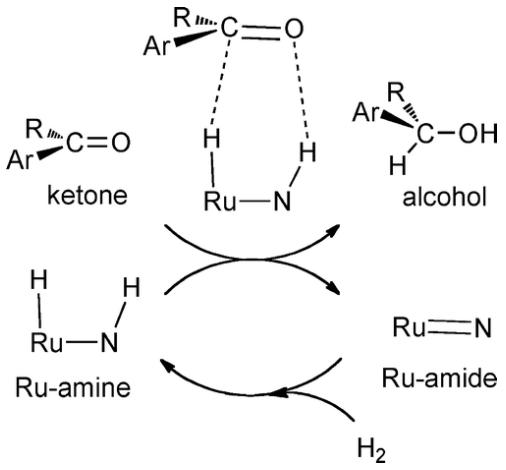


**Figure 1.10:** Outline of Noyori's bifunctional reaction mechanisms

Although 1-Ru is known to add $H_2$ via metal-ligand cooperation mechanism to form the octahedral 1-Ru-H, yet the exact mechanism of catalysis of 1-Ru has not been well understood (equation 1). Metal-ligand cooperation mechanism (MLC) is not restricted to the $H_2$ addition to 1-Ru; in fact, it has been reported in the chemical literature that numerous metal complexes, including catalysts, are known to proceed in the reaction pathway via a metal-ligand cooperation mechanism, where a part of the ligand is also involved in the mechanistic flow of the reaction. Such mechanisms involve a limited change in the structure of the ligands for the sake of activating the substrate and in turn forming the desired product. [19, 31]

Milstein and coworkers proposed an MLC mechanism that could be the key mechanism in catalysis.[8] They have assumed that the hydrogenation of esters and carboxamides to proceed by an MLC mechanism where the proton of the phosphine arm is transferred to the carbonyl oxygen of the substrate and the hydride is transferred to the carbonyl carbon resulting in hemiacetals or hemiaminals formations as intermediates in addition, 1-Ru being restored (equations 6 and 7). [32, 33]. They elaborate on the

issue, stating that the pincer complex first undergoes deprotonation at the pyridinyl methylenic carbon which gives rise to the dearomatized pyridine entity. The formed complex can then activate various chemical bonds, including but not limited to H—H, H—OH, H—OR, H—$NH_2$, H—$NR_2$, and H—C bonds. This reaction occurs by a cooperation mechanism between the metal and the ligand; at this stage, aromatization at the pyridine ring is regained as the octahedral 1-Ru-H is regenerated. The whole process does not involve any change in the oxidation state of the Ruthenium metal center. [3, 8, 26, 28]

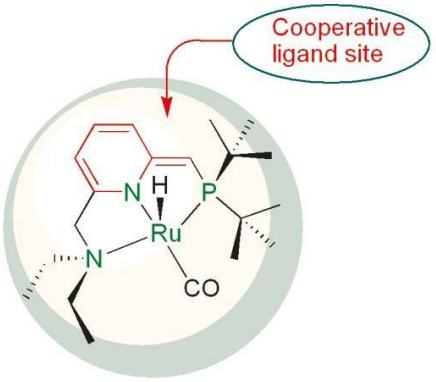


**Figure 1.11:** Top view of 1-Ru square pyramidal complex indicating the site of ligand cooperation (in red)

Milstein's suggested mechanism relates to the bifunctional mechanism reported by Noyori. Noyori's mechanism is known to proceed as a bifunctional hydrogenation in an outer sphere model without having the carbonyl functional group being coordinated to or in any interaction with the metal center. [29, 30]

To account for the complete hydrogenation of esters and carboxamides into alcohols and amines, the process requires a hydrogenolysis step of the C—OR bond or the C—NHR bond at some point in the reaction. Considering esters, and the hemiacetal intermediate would certainly fragment into an alcohol and an aldehyde even in a

complete absence of a catalyst (equation 8).[34] At a later stage, the aldehyde, in the presence of $H_2$ gas, would be hydrogenated by the present catalyst to give a second alcohol molecule. However, in the reaction of hydrogenation of carboxamides, hemiaminals are expected to undergo dehydrogenation reactions and transform into imines, the latter would be hydrogenated into amines depending on the reaction conditions and on the catalyst being used (equation 9). [10]

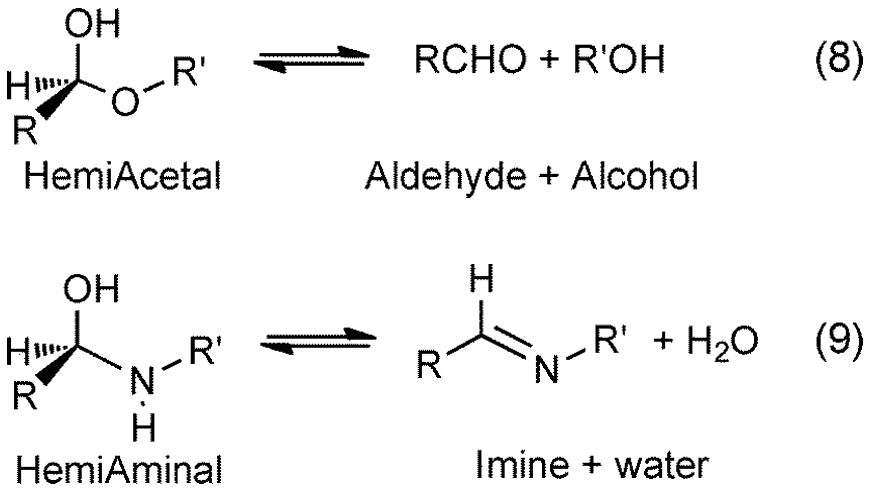


**Figure 1.12:** Equations (8) and (9) that demonstrate the dissociation of hemi acetals and hemiaminals

Depending on the catalyst and the reaction conditions, the imine can in turn be hydrogenated into a final amine product.[35-37] No imine or coupled amine products are observed in catalysis by 1-Ru. In a rather striking effect, however, when the PNP analogue of 1-Ru is used as the catalyst in amine coupling, imines are observed as the only products.[38] Significantly, although 1-Ru is a catalyst for alcohol coupling into esters, when it is used in the coupling of amines with alcohols, only carboxamides are observed as products.

The previously mentioned MLC mechanism has been taken into consideration by various computational studies. In a study by Wang and co., they investigated the

study of the amine coupling into carboxamides and suggest that the reaction would flow via metal ligand cooperation mechanism. Wang's mechanism begins in two preparatory steps: first steps is described as a dehydrogenation of the alcohol by 1-Ru catalyst to yield an aldehyde followed by an MLC addition of the N-H bond to 1-Ru to produce the octahedral ruthenium amide complex (2-Ru-NHR).[39]

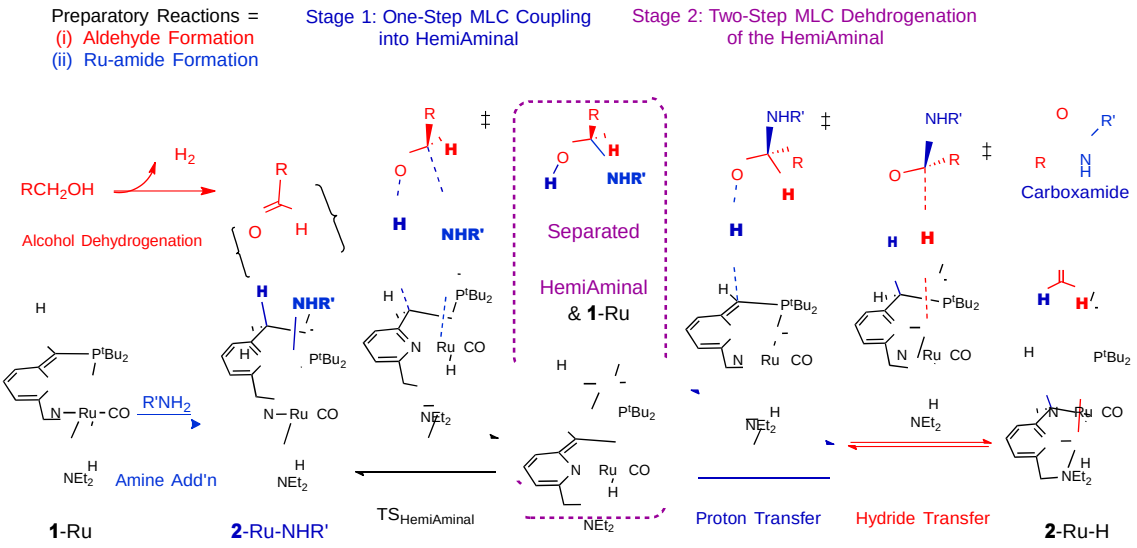


**Figure 1.13:** Outline of MLC mechanism for Amine-Alcohol coupling catalyzed by 1-Ru

After that, the formation of the carboxamide occurs in two stages, starting by a reaction between the aldehyde and Ruthenium-Amide (2-Ru-NHR) via formation of a six-member outer sphere ring transition state ($TS_{HemAm}$), this ring forms also via Metal ligand cooperation in which the Ru—N bond starts to break and the latter points out towards the carbonyl carbon, on the other hand, the pyridinyl methylenic proton is in the process of being abstracted by the Oxygen of the substrate. The products of this transition state are the separated hemiaminal and restoration of the 1-Ru catalyst. In the second stage of the reaction, 1-Ru and the produced hemiaminal react again in a two step reaction where at first a proton is transferred from the oxygen of the catalyst to the

phosphine arm of the catalyst, where the pyridine ring regains its aromaticity. The last step would involve a hydride transfer from the carbonyl carbon of the substrate to the

Ruthenium metal, giving off the final products: 1-Ru-H octahedral complex and a carboxamide.

## 2. Bifunctional Double Hydrogen Transfer Mechanism (BDHT)

Li and co performed another theoretical study for the same reaction pathway; they considered the formation of hemiacetals and hemiaminals as subsequent to the condensation of aldehydes that was produced from a dehydrogenative coupling of alcohols or of alcohol-amine systems without a need for a catalyst. After that, 1-Ru is thought to catalyze hemiaminals and hemiacetals dehydrogenation via sequential proton and hydride transfers that follow the metal ligand cooperation mechanism. In their studies, and if taken in the direction of esters and carboxamides, both Wang and Li would start by hydrogenation of the carbonyl into a hemiacetal or a hemiaminal; the divergence occurs in how hydrogenation takes place.[9, 39, 40]

For the alcohol dehydrogenation, Li and co. proposed a pathway that they referred to as Bifunctional Double Hydrogen Transfer (BDHT). Such mechanism goes as follows; the BDHT dehydrogenation mechanism is mediated by the bifunctional active site of 1-Ru that consists of a Lewis acidic Ru center and a Lewis basic $sp^2$ carbon center neighboring the phosphine arm of the pincer ligand. This step is very similar to the hydrogen transfer step that is thought to proceed by metal-ligand cooperation mechanism. [39, 40]

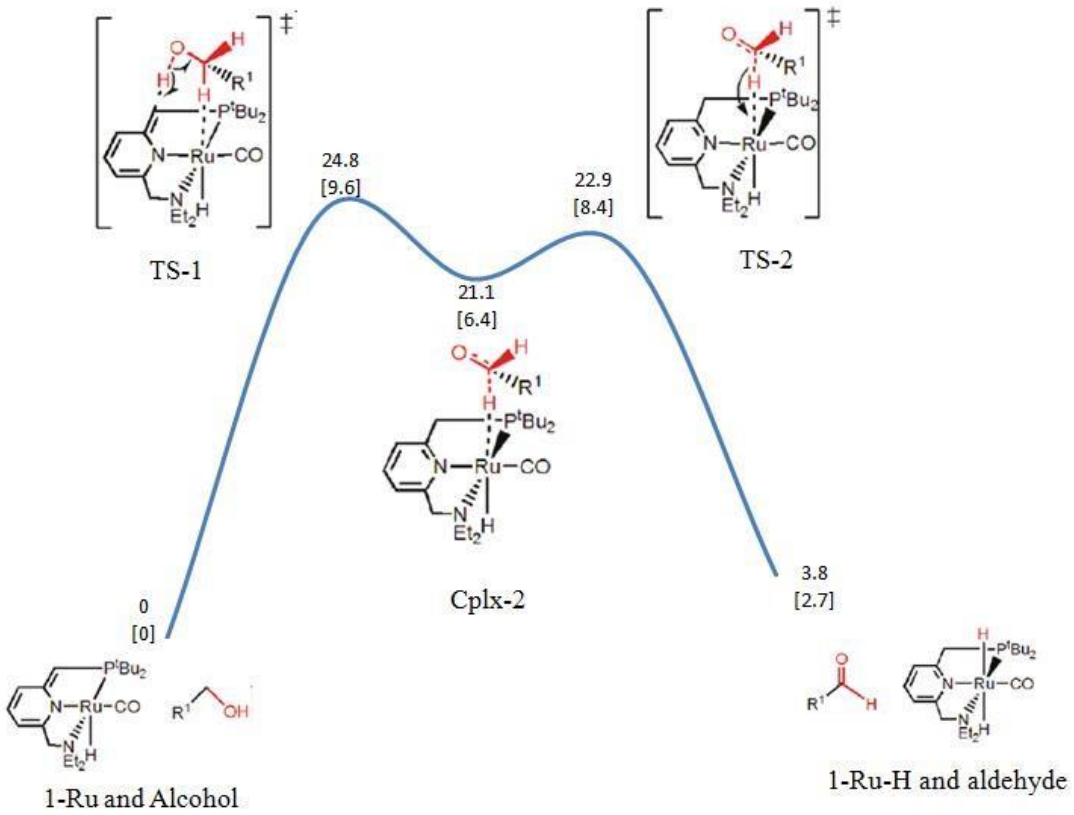


**Figure 1.14:** Potential Energy Surface of Alcohol dehydrogenation via bifunctional hydrogen transfer mechanism, values are given as ΔG [ΔH] and are reported in kcal/mol.

The BDHT pathway is shown to be a straight forward pathway in which the Ru metal center and the $sp^2$ carbon center serve as the hydride and the proton acceptors respectively. This double hydrogen transfer occurs via two steps, first a proton transfer from the oxygen to the carbon which proceeds via TS-1 (TS5 according to Li) transition state, this state shows the largest energy barrier, with a ΔG value of 24.8 Kcal/mol, rendering it the rate determining stage. This step is followed by a formation of an intermediate complex, Cplx-2 (12 according to Li), in which the Hydride is partially coordinated with the Ruthenium center and the aromatization of the pyridine ring is

gained as the hybridization of the carbon center changes from $sp^2$ to $sp^3$ by gaining a proton and the electron pair is donated to the pyridine ring. The second step would be the hydride transfer from the carbonyl carbon to the Ruthenium metal. This is shown on the potential energy diagram as TS-2 (TS6 according to Li). TS-2 has a relatively lower free energy value than TS-1 (22.9 kcal/mol compared to 24.8 kcal/mol, with a $\Delta\Delta G$ value of -1.9 kcal/mol). TS-2 paves the way to form the octahedral dihydride Ruthenium complex 1-Ru-H and a reactive aldehyde.

As for the hemiacetal/hemiaminal formations, Li and co. present a coupling mechanism where the aldehyde that has been formed in the previous stage would couple either with an amine to give a hemiaminal or with an alcohol to give a hemiacetal, both of which can undergo dehydrogenation at a later step to produce an amide and an ester respectively. After that, the hemiacetals/hemiaminals would undergo dehydrogenations to give off the desired esters or carboxamides respectively. As reported in their study, Li and co describe the reaction as being flowing according to Bifunctional Double Hydrogen Transfer mechanism that was described earlier. In a similar way to alcohol dehydrogenation reactions, both the hemiacetal and the hemiaminal (labeled as **14heac** and **13heam** respectively) undergo dehydrogenation stepwise. Also, the energy barrier, shown in the figure as the transition state **TS14** for the **13heam** dehydrogenation was found to be 27.3 kcal/mol relative to 1-Ru (**1cat** in Li's figure) and **13heam**. This value is very similar to the energy barrier for the dehydrogenation of hemiacetal (**TS16**) which was also reported to be 27.3kcal/mol relative to 1-Ru and **13heac**. The flow of the reaction in both ways starts with a proton transfer from the oxygen of the substrate to the $sp^3$ carbon of the phosphine arm. Again, aromatization is gained and this step is depicted in the diagram below as **TS14** for hemiaminal dehydrogenation and **TS 16** for

hemiacetal dehydrogenation. Both transition states would lead to octahedral complexes as intermediates, **30** and **31** in the figures, where the hydrogen of the carbonylic carbon is pointed towards the metal center. The step would be followed by a hydride transfer, shown as **TS15** and **TS17** in the diagram in which both would lead the octahedral Ruthenium dihydride complex 1-Ru-H (**5dih** according to Li's diagram) and either carboxamide **4amd** or ester **29est**.

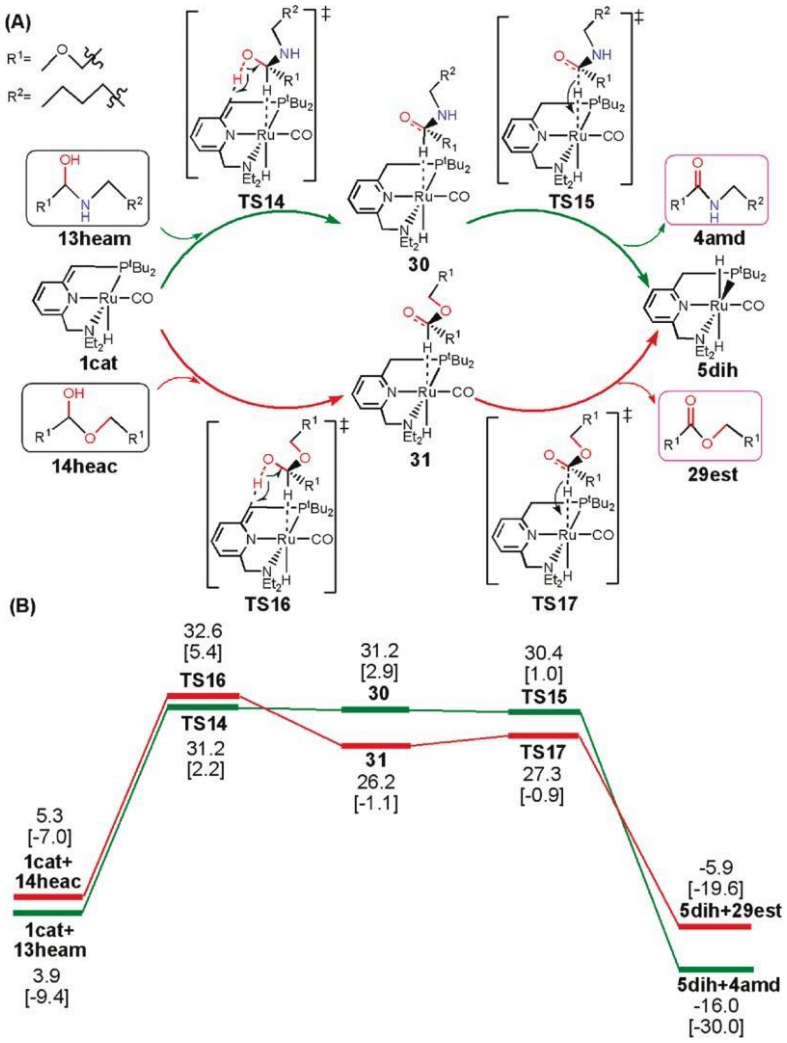


**Figure 1.15:** (A) Pathway for the dehydrogenation of the hemiacetals/hemiaminals intermediates via BDHT and (B) the corresponding energy profiles reported as ΔG [ΔH] in kcal/mol[41]

Li and co. have presented a thorough computational study on the role of Ru(II)-PNN pincer ligand in the hydrogenation of alcohols and amines into esters and carboxamides. Their presented bifunctional double hydrogen transfer mechanism is a similar approach to the earlier described Metal-ligand cooperation mechanism in which the ligand would directly interfere and aid the metal in catalysis.[9]

### G. Proposed Direct Route Metathesis Mechanism

Herein, and using electronic structure DFT methods, we investigate alternative, more direct H/OR and H/NHR metathesis routes to the alcohol/amine coupling that circumvent the intermediacy of hemiacetals or hemiaminals. The newly proposed mechanism involves formation of hemiacetaloxide and hemiaminaloxide ion-pairs by addition of an aldehyde (from metal-catalyzed alcohol dehydrogenation) to an octahedral ruthenium-alkoxide or ruthenium-amide intermediate (from alcohol or amine addition to 1-Ru), followed by simple rearrangement (slippage) within the intact ion-pairs to transfer a hydride from the hemiacetaloxide or hemiaminaloxide to the metal. We show that the computed potential energy surfaces that are sometimes invoked to support the MLC mechanism correspond to indirect routes to metathesis. Both the ion-pair and the MLC routes predict the dehydrogenative coupling of ethanol and methanol into methyl acetate to be kinetically much more favored than the kinetics of formation of N-methylacetamide from ethanol and methylamine. However, the calculations provide evidence for the accessibility of a low energy NHR/OR metathesis path that would amidate the ester into the experimentally observed thermodynamically more favored carboxamide product.

## H. Computational Methods and Solvation Models

This study was done on the dimethyl amino analogue of 1-Ru, but for convenience we use the same notation for both systems. All calculations were carried out using Gaussian 09. [42] Geometry minimization and normal mode vibrational analysis were done in the gas phase at the M06 level,[43] using the 6-31++G(d,p) basis set on the nonmetal elements, and the Hay−Wadt relativistic effective core potential (ECP) on ruthenium[44, 45], along with a double-ζ basis set augmented with one f polarization and one diffuse d function (exponents = 1.24 and 0.015, respectively) [46]. Selected transition states were also used to conduct intrinsic reaction coordinate analysis (IRC) [47]. Final electronic energies were obtained using the gas phase geometries at the M06, M06L, [48] and ωB97X-D [49] levels of theory which are among the more popular methods used in computational organometallic chemistry. For this purpose the larger 6-311++G(2d,2p) basis set was used on the nonmetal elements, and an additional f polarization function with exponent = 0.4 was added to Ru. The reported standard state Gibbs free energies were obtained at 298 K and 1 atm using the entropies from the gas phase calculations after scaling them by a factor of 0.5. The reason for scaling the entropies in associative reactions is discussed in the studies by Wang where he based his scaling on experimental results. [38] The scaling factor influences the absolute free energies of the transition states of interest but does not change the main conclusions of the study.

Experimentally, much of the hydrogenation and coupling chemistry of 1-Ru had been done using toluene as solvent, though some experiments had been also carried out in THF, dioxane, DMSO, and anisole, or without a solvent. [11, 12] In the present study two approximation levels are applied to model the solvent. In one, bulk solvent

effects are included using the SMD model [50], with toluene, THF, or methanol as the solvent continuums. Because alcohols are either reactants or products in the reactions of interest, the second approximation level includes a methanol molecule explicitly in the calculations (along with the solvent continuum) to mimic possible specific H-bonding interactions.

# CHAPTER II

# DIRECT OUTER-SPHERE METATHESIS MODEL: DFT RESULTS

## A. Computed Reaction Energies of 1-Ru

The reactions of the square pyramidal **1**-Ru with $H_2$, methanol, and methylamine (eqs 10–12) are of central importance to the present study. In Table 1 we compare the free energies of the three reactions computed using the M06, M06L, and ωB97X-D density functionals and in different solvent continuums. The values given in the equations are for the M06L-toluene results.

$$\textbf{1}\text{-Ru}+H_2 \rightleftharpoons \textbf{2}\text{-Ru-H} \quad \begin{matrix}\Delta H^\circ = -11.4;\ \Delta S^\circ = -16.2\ \text{eu} \\ \Delta G^\circ = -6.6\ \text{kcal/mol}\end{matrix} \tag{10}$$

$$\textbf{1}\text{-Ru}+\text{MeOH} \rightleftharpoons \textbf{2a}\text{-Ru-OMe} \quad \begin{matrix}\Delta H^\circ = -11.8;\ \Delta S^\circ = -22.6\ \text{eu} \\ \Delta G^\circ = -5.0\ \text{kcal/mol}\end{matrix} \tag{11}$$

$$\text{1-Ru}+\text{MeNH}_2 \rightleftharpoons \textbf{2a}\text{-Ru-NHMe} \quad \begin{matrix}\Delta H^\circ = 0.0;\ \Delta S^\circ = -22.7\ \text{eu} \\ \Delta G^\circ = +6.8\ \text{kcal/mol}\end{matrix} \tag{12}$$

| | **$H_2$** | **MeOH** | **$MeNH_2$** |
|---|---|---|---|
| **M06 (toluene)** | –3.9 | –1.4 | +10.5 |
| **M06L (toluene)** | **-6.6** | **-5.0** | **+6.8** |
| **ωB97X-D (toluene)** | –7.1 | –3.5 | +8.4 |
| **M06L (THF)** | –7.5 | –3.0 | +8.7 |
| **M06L (methanol)** | –7.7 | –2.4 | +10.8 |

**Table 1.** Computed $\Delta G^o$ of $H_2$, Methanol and Methylamine Addition to **1**-Ru, Results from single-point calculations in a polarizable solvent continuum using geometries minimized in the gas phase at the M06 level.

The three methods predict $H_2$ addition to **1**-Ru to be exoergic by 3.9–7.1 kcal/mol ($\Delta G^o$ at 298.15K and 1.0 atm). The results are qualitatively consistent with the observation that **1**-Ru adds $H_2$ readily to give an isolable ruthenium trans-dihydride product. Solutions of 1-Ru in benzene are also known to react with few equivalents of methanol to give an octahedral ruthenium alkoxide, but this product could not be isolated as a solid. The different methods in Table 1 predict methanol addition to 1-Ru to be approximately 2 kcal/mol less exoergic than $H_2$ addition. Finally all of the methods in Table 1 agree that the thermodynamics of methylamine addition to 1-Ru should be about 12 kcal/mol less favored than methanol addition.

The energies in Table 1 exhibit small dependencies on the choice of the solvent continuum in the calculations. For $H_2$ addition, changing the continuum from toluene to THF or methanol favors the reaction by ~1 kcal/mol. In contrast, THF and methanol disfavor methanol and methylamine addition by more than 2 kcal/mol.

For the three reactions in Table 1, the M06 energies are significantly less exoergic than either the M06L or the ωB97X-D ones. As mentioned above, the free energies in Table 1 are obtained after scaling the gas phase entropies by a factor of 0.5. This value is arbitrary and probably exaggerated. If the entropies were scaled by 0.7, $\Delta G^o$ for methanol addition in toluene at the M06 level would be +1.2 kcal/mol, which would be inconsistent with the experiment. With a scaling factor of 0.7, the M06L and ωB97X-D energies remain exoergic by 2.3 and 0.8 kcal/mol, respectively. Studies by Truhlar[51] and more recently by Gusev[52] (using different basis sets than the ones employed here) showed the M06L functional to be systematically accurate in reproducing experimental enthaplies of organometallic reactions having different

characters. A recent theoretical investigation of agostic bonding in nickel complexes by Pudasani and Jenesko showed the M06L results to be in good agreement with those from the high level correlation consistent composite approach for transition metals.[53] Similarly, a comprehensive benchmark study by Remya and Suresh of noncovalent interactions between polar molecules found the M06L functional to be the "best performer" in a comprehensive pool of density functionals.[54] The latter systems are directly relevant to the type of potential energy surfaces elucidated in the present study. Accordingly, we chose to base the discussion in the present work on the M06L energies (with the 0.5 entropy scaling factor), and at the end we give a table that compares the relative energy of the key transition states at different levels and in different solvents. We note that we had completed geometry minimization at the M06 level before the given method-validation studies were published. We verified for select reactions that the same final energies are obtained if the geometries were minimized at the M06L or ωB97X-D levels.

### B. Metathesis in the Hydrogenation Direction

Although the ultimate interest of the present study is the dehydrogenative coupling of alcohols and amines, we find it most useful to approach the problem from the hydrogenation direction starting with the octahedral **2**-Ru-H. Because we are largely after supporting the plausibility of a new reaction mode for the C–OR or C–NHR bond-making or -breaking step in a complex multistage reaction system, we chose to work with the simplest ester and carboxamide, namely methyl acetate (**3**) and *N*-methylacetamide (**4**). Due to the asymmetry of the PNN ligand the two hydrides in **2**-Ru-H are not equivalent. This allows definition of several stereoisomeric outer-sphere pathways in the reaction of **2**-Ru-H with a carbonyl compound[55, 56]. We focus on the

pathway that aligns the carbonyl of **3** or **4** along the ruthenium–amine bond of **2**-Ru-H (defined as path **a**) as illustrated in equation 13 for the precomplex between **2**-Ru-H and **3**.

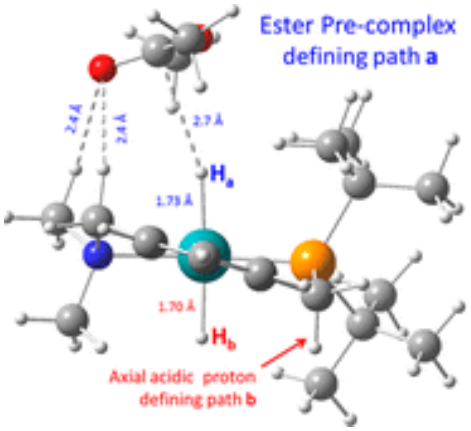


(13)

On this path the carbonyl oxygen is on the opposite side of the axial methylene proton of the phosphine arm that is needed in metal–ligand cooperation, which we denote as path **b** and will be discussed later. The structural and energy data for the stationary points identified on path **a** are given in Figure 2.1.

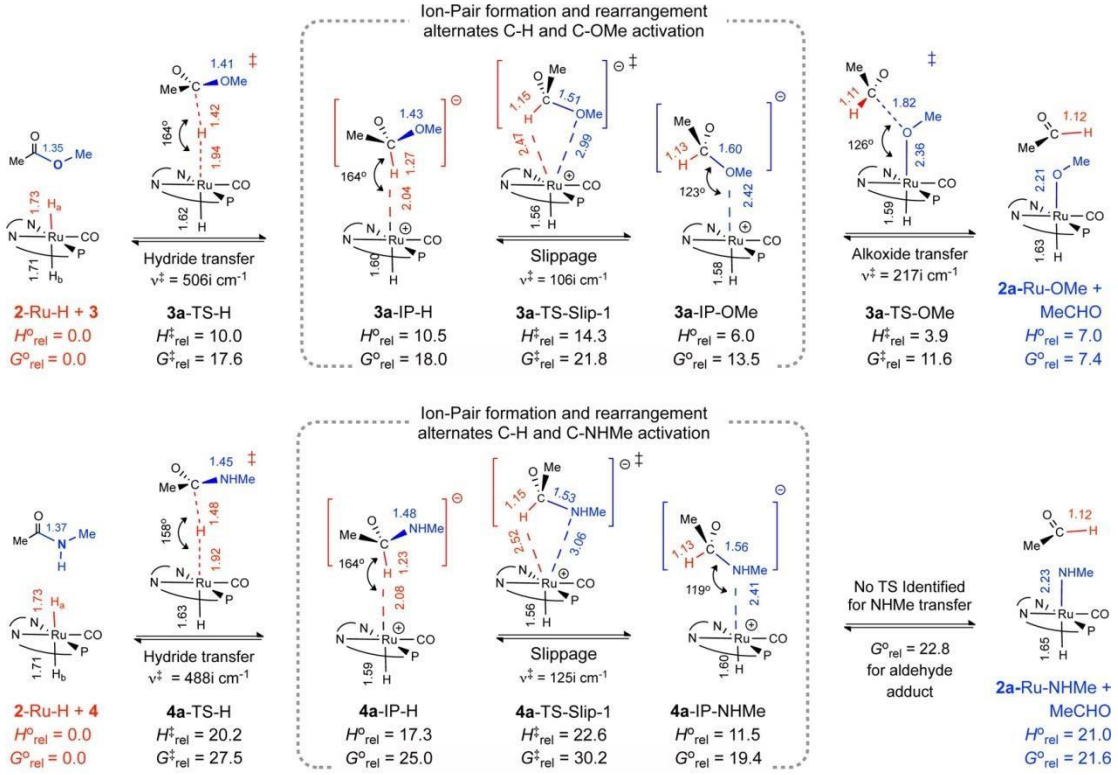


**Figure 2.1**. Stationary points on the outer-sphere PES in the reaction of an ester (**3**) and a carboxamide (**4**) with **2**-Ru-H. Energies are given in kcal/mol relative to the separated reactants (M06L-toluene SMD continuum).

The PES in Figure 2.1 starts with a transition state (**3a**-TS-H) for hydride transfer characterized by a Ru–H and C–H bond distance of 1.94 and 1.42 Å; respectively, and an imaginary frequency of 506i $cm^{-1}$. **3a**-TS-H leads to an ion-pair minimum between a hemiacetaloxide and a square pyramidal ruthenium cation in which the C–H bond is pointed to the metal at 2.04 Å (**3a**-IP-H). The C–H bond of the hemiacetaloxide anion in **3a**-IP-H is long (1.27 Å), implicating some degree of activation due to metal coordination. The proposed H/OR metathesis pertains to rearrangement of the ion-pair to coordinate the OMe group of the hemiacetaloxide to the metal in place of the α-hydrogen. The PES has a minimum for the latter species (**3a**-IP-OMe) characterized by a relatively long Ru–OMe bond (2.42 Å), and, more

importantly, a significant stretch of the C–OMe bond to 1.60 Å. The computed stretch implies that coordination of the OMe group to the metal activates the C–OMe bond just as it does for the C–H bond in **3a**-IP-H. From **3a**-IP-OMe, the gas phase calculations identify a TS for C–OMe cleavage (**3a**-TS-OMe) that mirrors the hydride transfer TS. **3a**-TS-OMe can be thought to "transfer" an alkoxide from the hemiacetaloxide to the metal to give the octahedral **2a**-Ru-OMe and eliminate acetaldehyde.

The net reaction of **3** in Figure 2.1 is a metathesis exchanging a hydride and an alkoxide between the metal center of **2**-Ru-H and the acyl group of the ester. The given reaction requires a "mechanism" to alternate the coordination of the C–H and C–OMe groups of the hemiacetaloxide to the metal. In Figure 2.1 we consider a transition state (**3a**-TS-Slip-1) that achieves the rearrangement in a direct way within the intact ion-pair by pointing both the α-H and the OMe groups of the hemiacetaloxide to the metal. The Ru–H (2.47 Å), C–H (1.13 Å), C–OMe (1.51 Å) and Ru–OMe (2.99 Å) parameters in **3a**-TS-Slip-1 are all intermediate between the corresponding values in the C–H and C–OMe ion-pair. The 3-D molecular displays given in Figure 2.2 reveal a good structural fit of the hemiacetaloxide in the catalyst "cavity" in each of the three TSs on the metathesis PES.

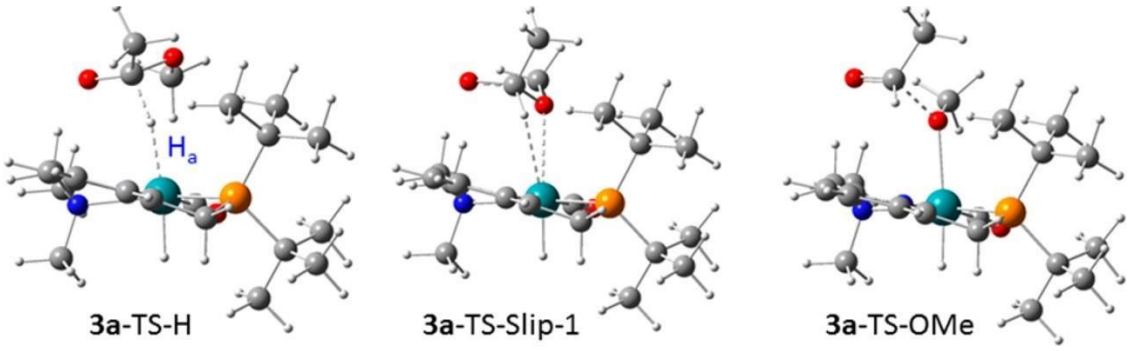


**Figure 2.2:** Molecular displays of the three TSs on the metathesis PES of **3**

The computed enthalpy and free energy of the precomplex between the ester and **2**-Ru-H in equation 13 are −3.5 and 3.9 kcal/mol, respectively (M06L, in toluene continuum). The barrier for hydride transfer relative to the separated reactants is 17.6 kcal/mol. This is a relatively low barrier, a result that can be attributed to two factors: (i) an electronic one following from the trans-configuration of the two hydrides in **2**-Ru-H, [55, 56] and (ii) a structural factor following from the presence of an opening over the amino group which clearly a llows the ester to approach the hydride without much steric demand (Figure 2.2). The C–H bound ion-pair minimum has an energy nearly identical to that of **3a**-TS-H, and from this point the barrier to rearrangement via **3a**-TS-Slip-1 is only 3.8 kcal/mol. The OMe bound ion-pair is 4.5 kcal/mol more stable than **3a**-IP-H, which seems consistent with the better coordinating ability of an OMe group compared to a C–H bond. From **3a**-IP-OMe the gas phase M06 electronic barrier to C–OMe cleavage via **3a**-TS-OMe is just 0.5 kcal/mol. IRC calculations in the gas phase starting from **3a**-TS-OMe confirm the connectivity (Figure 2.3) and supports the near absence of a barrier. The barrier for C–OMe dissociation becomes slightly negative when the thermal enthalpic terms and solvent effects are included via single point M06L calculations.

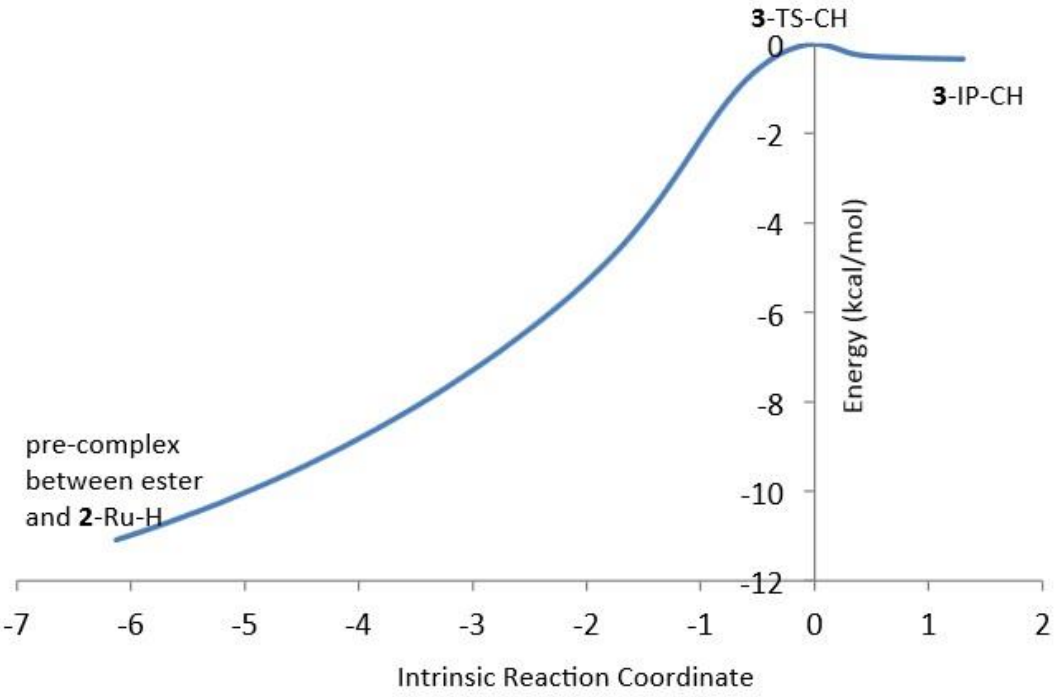


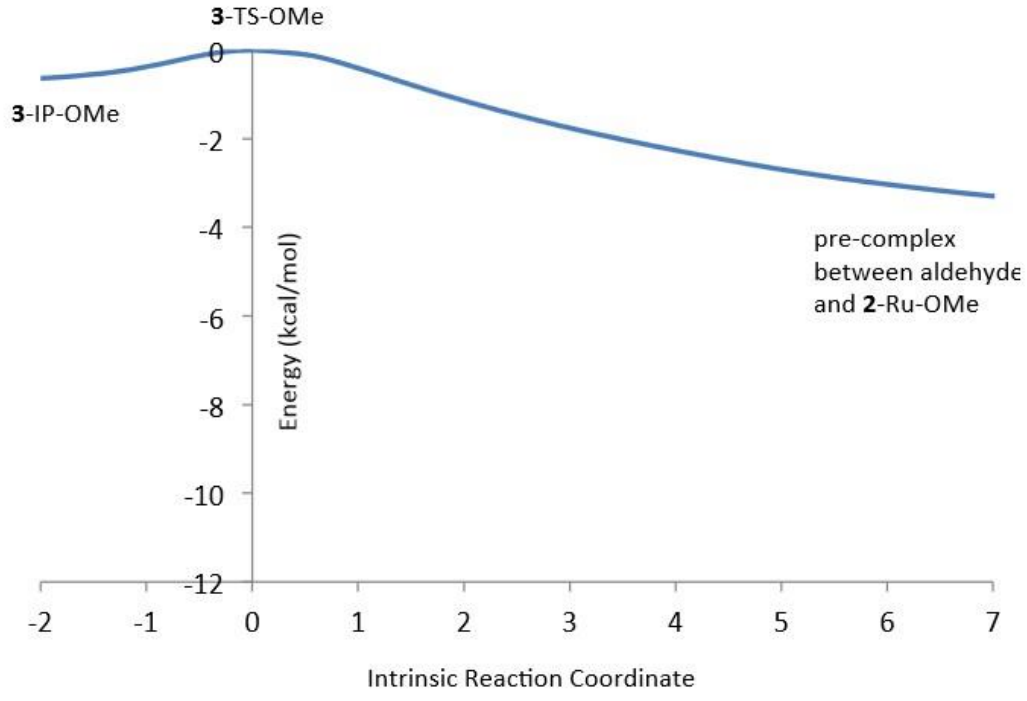


**Figure 2.3:** Intrinsic Reaction Coordinates plots starting from3-TS-H and 3-TS-OMe

In fact, for many of the other stereoisomeric paths the calculations failed to identify a TS for C–OMe cleavage due to the flatness of the PES of the C–OMe cleavage step. We recommend that a relaxed scan of the PES as a function of the C–OR bond distance is used before seeking to identify TSs related to **3a**-TS-OMe. Complete aldehyde elimination from **3a**-IP-OMe is exoergic by 6.1 kcal/mol. The similar energy of each C–H and OMe ion-pair and the corresponding C–H and C–OMe TS indicates that the given ion-pairs themselves can be viewed as activated species on the PES, meaning that once the hydrogen or the OMe group of the α-carbon of the hemiacetaloxide gets into the vicinity of the metal center, it will undergo a barrierless downhill C–H or C–OMe cleavage (corresponding, respectively, to hydride or alkoxide transfer to the metal). Under this condition, **3a**-TS-Slip-1 is the highest energy point on the metathesis PES with $G^{\ddagger}_{rel}$ = 21.8 kcal/mol relative to the separated reactants. This means the direct ion-pair mediated H/OR metathesis of esters can be a chemically relevant reaction even at ambient temperatures.

As found for the ester, the PES in the reaction between *N*-methylacetamide (**4**) and **2**-Ru-H in Figure 2.1 also starts with a precomplex followed by a hydride transfer TS (**4a**-TS-H) leading to a C–H bound hemiaminaloxide ion-pair minimum (**4a**-IP-H). The barrier for hydride transfer to **4** is much larger than in the reaction of **3**. As found for the ester, the energy of the TS and the C–H ion-pair minimum of **4** are close: 27.5 and 25.0 kcal/mol, respectively.

A "stepwise" ion-pair mediated metathesis starting with the carboxamide requires coordination of the amino nitrogen of the hemiaminaloxide to the metal. A minimum for the latter species (**4a**-IP-NHMe; Figure 2.1) is computed to have $G^{o}_{rel}$ = 19.4 kcal/mol, a full 5.6 kcal/mol *lower* than the preceding C–H bound ion-pair, which

is reasonable, given that the amino group is a classical two-electron donor ligand. In spite of the favorable thermodynamics, however, the barrier for the direct slippage step from **4a**-IP-H to **4a**-IP-NHMe via **4a**-TS-Slip-1 is 5.2 kcal/mol, slightly larger than the matching barrier for hemiacetaloxide slippage (3.8 kcal/mol). The TS structures suggest the difference could follow from slightly greater steric demands in **4a**-TS-Slip-1 due to the additional hydrogen of the NHMe group. With an increased energy input in both the hydride transfer and the slippage components of the H/NHMe metathesis, $G^{\ddagger}_{rel}$ of **4a**-TS-Slip-1 comes to 30.2 kcal/mol. This is a quite substantial barrier, but it is still not prohibitive for the reaction to be chemically relevant under the conditions used in the hydrogenation of carboxamides, which are typically done at temperatures greater than 100 °C and reaction times in the hours.

Upon slippage from **4a**-IP-H to **4a**-IP-NHMe the C–H bond of the hemiaminaloxide contracts from 1.23 to 1.13 Å, whereas the C–NHMe bond lengthens from 1.48 to 1.56 Å. This suggests that coordination of the amino group to the metal weakens the C–NHMe bond, but not to the same extent computed for C–OR activation. However, full C–NHMe bond cleavage starting from **4a**-IP-NHMe into the separated acetaldehyde and the octahedral **2**-Ru-NHMe products is calculated to be highly *endothermic* ($\Delta H^{o}_{Diss}$ = 9.5 kcal/mol). Thus, even with the favorable dissociation entropy term (scaled by 0.5) acetaldehyde elimination from **4a**-IP-NHMe is uphill by 2.2 kcal/mol. This behavior is fundamentally different from C–OMe cleavage, where the corresponding $\Delta H^{o}_{Diss}$ and $\Delta G^{o}_{Diss}$ starting from **3a**-IP-OMe were 1.0 and −6.1 kcal/mol, respectively. The different thermodynamics of the C–OMe and C–NHMe cleavage reactions raises questions on whether the kinetics of the C–NHMe will encounter an increased barrier or not. As shown in Figure 2.4, C–NHMe cleavage leads

at first to an adduct between acetaldehyde and the octahedral **2a**-Ru-NHMe characterized by an N–C bond distance of 2.91 Å. The transformation from ion-pair **2a**-Ru-NHMe to the adduct is uphill by 3.4 kcal/mol. Our extensive attempts to identify a TS for C–NHMe cleavage from **4a**-IP-NHMe to the adduct have not been successful. A relaxed PES scan as a function of the C–NHMe bond distance supports the absence of any significant barrier to dissociation beyond the uphill thermodynamics. Thus, in Figure 2.1 we use the energy of the aldehyde adduct ($G^{o}_{rel}$ = 22.8 kcal/mol) as a rough estimate for the energy of the missing **4a**-TS-NHMe. On the basis of the given results we can conclude that the slippage TS is the highest energy point on the direct H/NHMe metathesis PES in Figure 2.1.

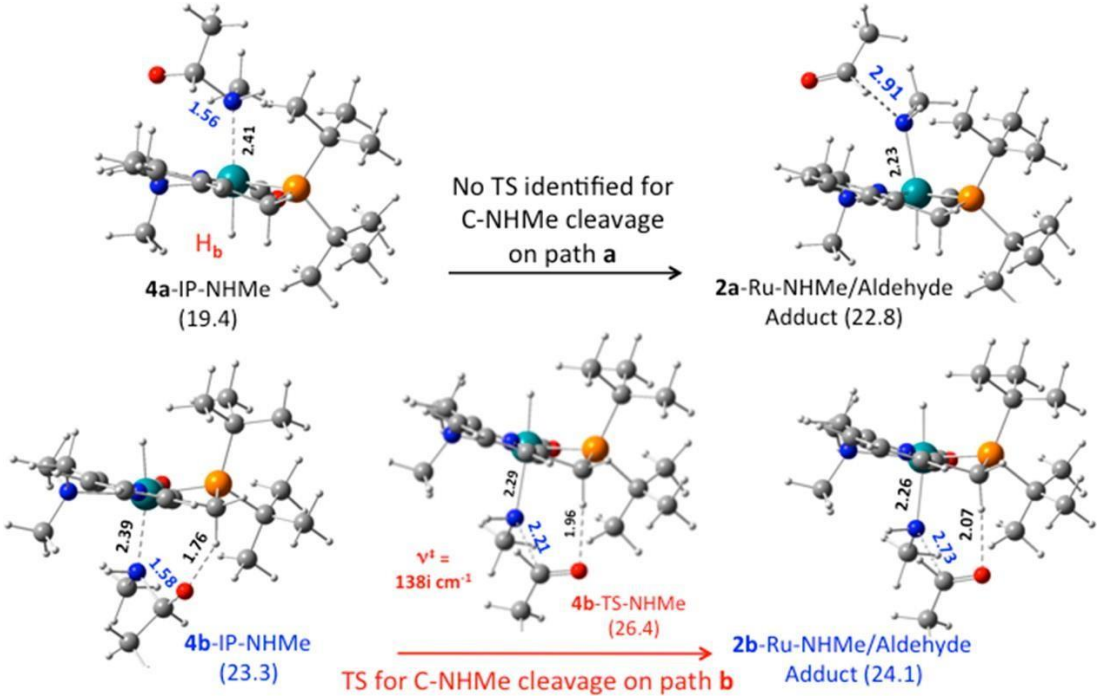


**Figure 2.4:** Comparison of C–NHMe bond cleavage of the amine-bound hemiaminaloxide ion-pair on paths **a** and **b**. Energies are given in kcal/mol, and distances in Å.

Further investigation of the question of the barrier of the metal-mediated C–NHMe cleavage starting from a higher energy ion-pair on path **b** (**4b**-IP-NHMe; $G^{o}_{rel}$ = 23.3 kcal/mol) identified a TS for C–NHMe cleavage characterized by a C–NHMe bond distance of 2.21 Å and an imaginary frequency of 138i $cm^{-1}$ (**4b**-TS-NHMe; Figure 2.4). As found on path **a**, C–NHMe cleavage on path **b** leads to an aldehyde adduct of **2b**-Ru-NHMe as a true minimum on the PES but with a slightly higher energy than the adduct on path **a** ($G^{o}_{rel}$ = 24.1 vs 22.8 kcal/mol). Overall, the given data indicate that formation and cleavage of the amine-bound hemiaminaloxide ion-pair on path **b** should be much less favored than that on path **a**. Nevertheless, $G^{\ddagger}_{rel}$ of **4b**-TS-NHMe comes to 26.4 kcal/mol relative to the separated reactants, which is still significantly lower than that of **4a**-TS-Slip-1 on path **a** (30.2 kcal/mol; M06L). We note however that at the ωB97X-D level the energies of the slippage (path **a**) and C–N cleavage (path **b**) TSs become equal ($G^{\ddagger}_{rel}$ = 29.6 kcal/mol). Note that on path **b** the carbonyl oxygen gets close to the axial proton of the phosphine arm (1.76 Å in **4b**-IP-NHMe and 1.96 Å **4b**-TS-NHMe), but there is no indication of any active role of the ligand in assisting C–NHMe cleavage. In addition, the significantly higher energy of **4b**-IP-NHMe compared to that of **4a**-IP-NHMe (3.9 kcal/mol) suggests an absence of a stabilizing bonding CH–carbonyl interaction.

### C. Intrinsic Reaction Coordinates

To further characterize the PESs elucidated above we conducted IRC analyses starting from **3a**-TS-Slip-1 and **4a**-TS-Slip-1. The calculations were carried out in the gas phase at the same (M06) level used in geometry minimization. The M06 electronic energy along the two IRCs relative to the TSs is plotted in Figure 2.5. The figure includes 3-D molecular displays of the C–H and C–OMe ion-pairs extracted from the

actual IRC outputs. The results confirm that TS-Slip-1 mediates a direct connection between C–H and C–OMe or C–NHMe "rotamer" ion-pairs. The structural parameters along the two IRCs starting from the C–H ion-pair side reveals smooth contraction of the C–H bond along with a smooth elongation of the C–OMe or C–NHMe bond as TS-Slip-1 is reached and crossed. Finally, the plots reveal a quite flat region of the PES around each of the slippage TSs, which is consistent with the small magnitude of the imaginary frequency in **3a**-TS-Slip-1 and **4a-TS-**Slip-1: 106i and 125i $cm^{-1}$, respectively.

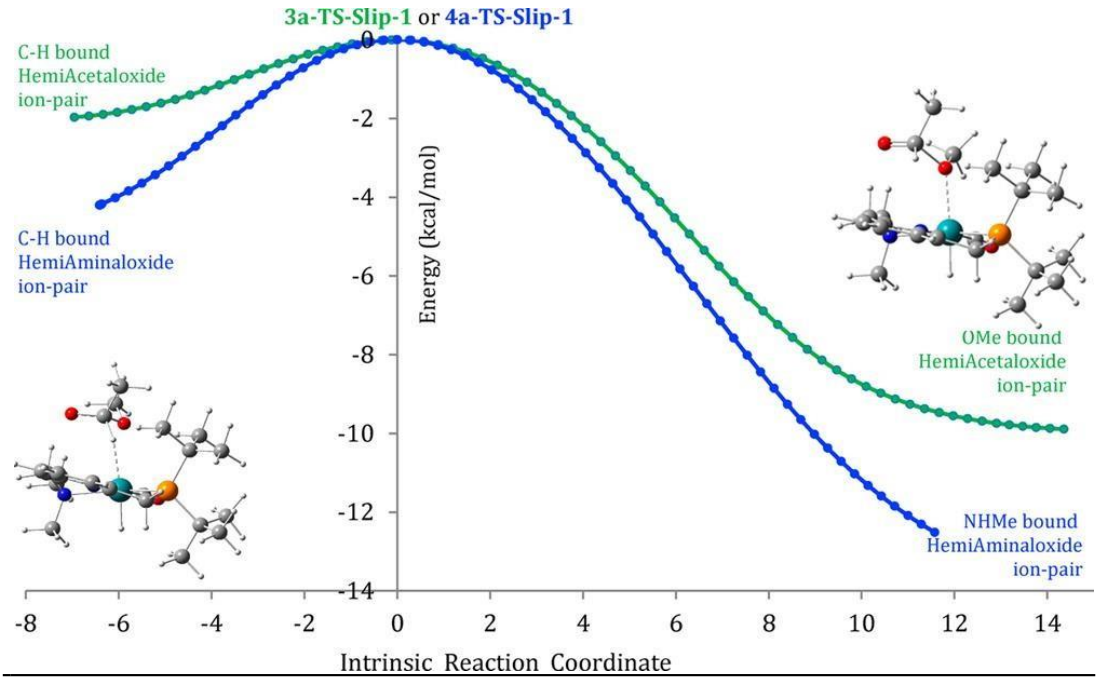


**Figure 2.5.** IRCs originating from **3a**-TS-Slip-1 (green curve) and **4a**-TS-Slip-1 (blue curve). M06 gas phase electronic energies are defined relative to the TSs in kcal/mol.

### D. Energy Profiles for full Hydrogenation

Figure 2.6 compares the Gibbs free energy profiles for complete hydrogenation of **3** and **4**. For convenience, the thermodynamics data for the individual hydrogenation and hydrogenolysis steps are collected in figure 2.7.

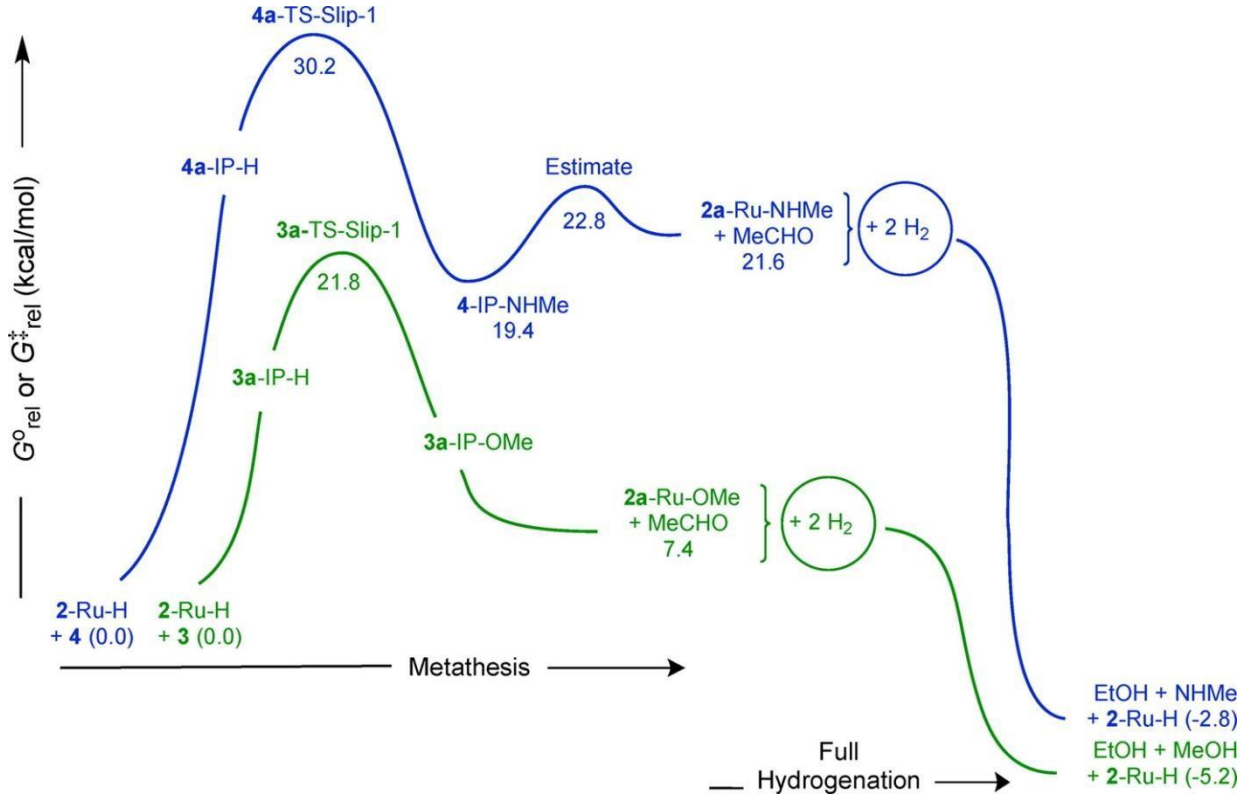


**Figure 2.6.** Gibbs free energy profiles (298 K and 1 atm) for the hydrogenation of **3** and **4** using **2**-Ru-H (M06L-toluene; in kcal/mol).

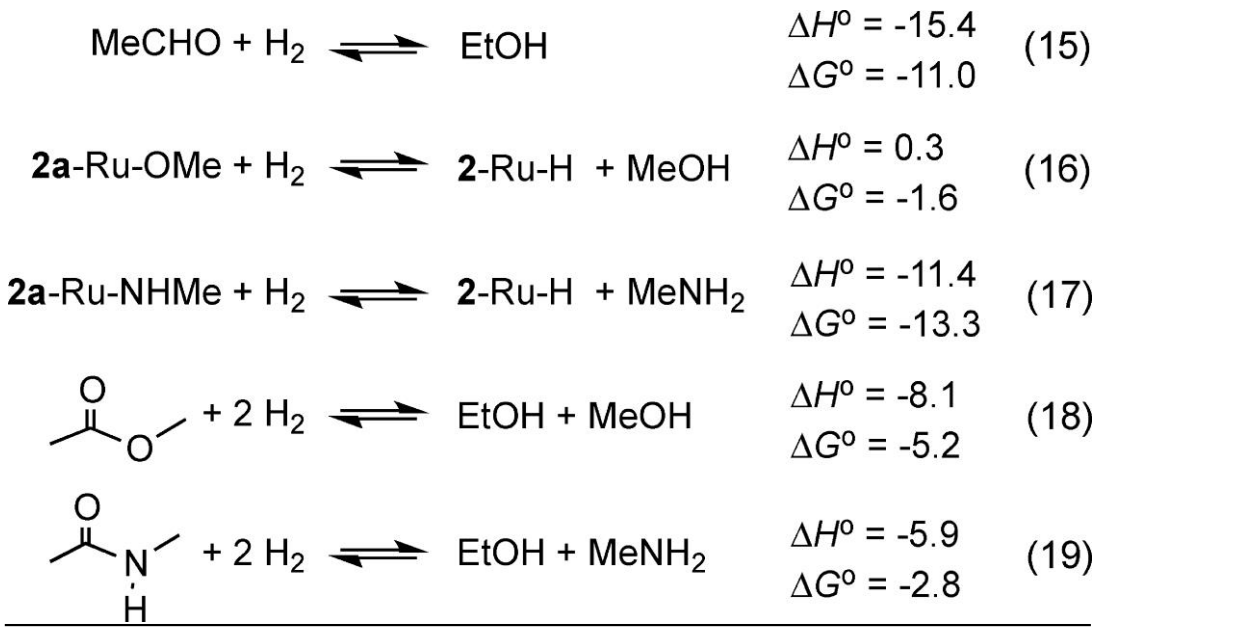


**Figure 2.7.** Computed Thermodynamics Data Used in Figure 2.6 (M06L-Toluene; in kcal/mol)

The metathesis in the direction of acetaldehyde formation from **3** and **4** is endoergic by 7.4 and 21.6 kcal/mol, respectively. However, hydrogenation of acetaldehyde is exoergic by 11.0 kcal/mol (eq 15 in figure 2.7), so it provides a major component in driving the hydrogenation thermodynamics of both the ester and the carboxamide.

For complete hydrogenation and catalysis the octahedral **2a**-Ru-OMe and **2a**-Ru-NHMe products must undergo hydrogenolysis to produce an alcohol or an amine and regenerate **2**-Ru-H. These reactions are exoergic by 1.6 and 13.3 kcal/mol, respectively (Table 1 and equations 16 and 17 in Figure 2.7). With these computed energies, the net hydrogenation of methyl acetate and *N*-methylacetamide comes to be exoergic by 5.2 and 2.8 kcal/mol, respectively (equations 18 and 19 in Figure 2.7).

Mechanistically, hydrogenolysis of the Ru–OR and Ru–NHR bonds can proceed in several routes including initial MLC elimination of the alcohol or the amine followed by $H_2$ addition to the square pyramidal **1**-Ru, direct hydrogenolysis with $H_2$,[57] and solvent-assisted mechanisms.[58-62] Given the highly favorable thermodynamics and the accessibility of many reaction routes, hydrogenolysis of the Ru–OMe and Ru–NHMe bonds is not expected to be kinetically demanding. Similarly, in the presence of **2**-Ru-H (which should be abundant under high $H_2$ pressure) hydrogenation of the aldehyde is expected to be fast. For simplicity we keep the barriers for aldehyde hydrogenation out of the PESs in Figure 2.6. The important point for our purposes is that Figure 2.6 gives unambiguous evidence that the metathesis route to hydrogenation should be kinetically and thermodynamically much more favored for **3** than for **4**. This may sound trivial since it is well-known that carboxamides are

generally much harder to hydrogenate than esters.[63] However, accepting the large differences in the hydrogenation PESs becomes critical in the coming discussion of the origin of the observed selectivity to carboxamides over esters in the dehydrogenative coupling of alcohols and amines.

### E. Metathesis via carbonyl insertion and deinsertion

The slippage TSs in Figure 2.1 alternate the coordination of the C–H bond of a hemiacetaloxide or hemiaminaloxide with an alkoxy or amino group. In Figure 2.8 we consider another ion-pair rearrangement mode via TS-Slip-2 to coordinate the terminal C–O$^-$ bond of the hemiacetaloxide or hemiaminaloxide to the metal.

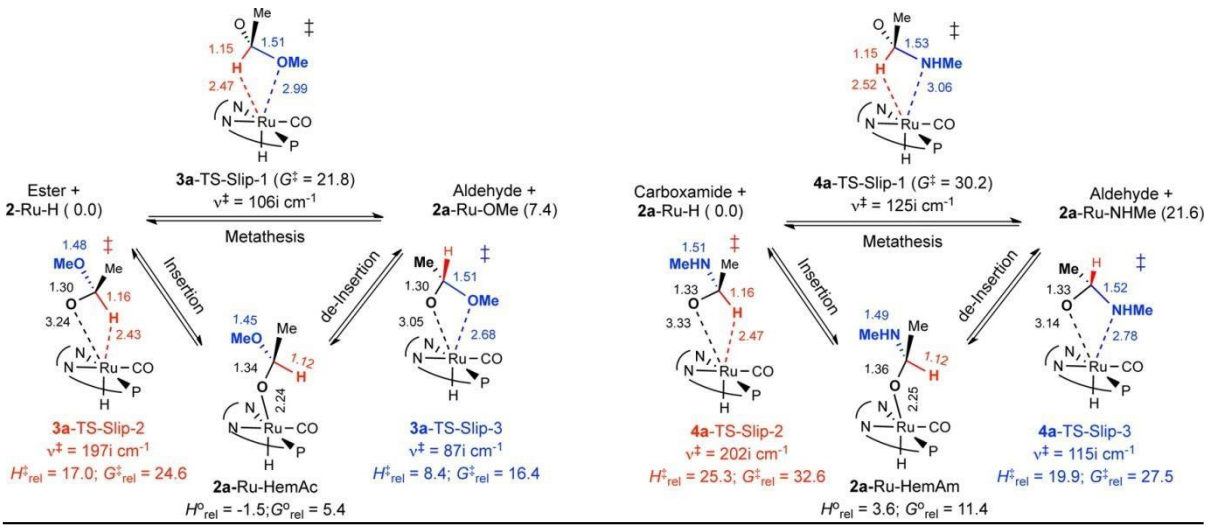


**Figure 2.8**. Three ion-pair-mediated reactions. The energies are given in kcal/mol relative to the separated **2**-Ru-H and **3** or **4**.

The new slippage mode leads to octahedral Ru–hemiacetaloxide and Ru–hemiaminaloxide complexes, **2a**-Ru-HemAc and **2a**-Ru-HemAm, respectively, having Ru–OR bond distances of 2.24 Å, close to the value of 2.21 Å for the Ru–OMe bond in **2a**-Ru-OMe (Figure 2.1). A molecular display of **2a**-Ru-HemAc is given in equation 20 (without the *tert*-butyl groups).

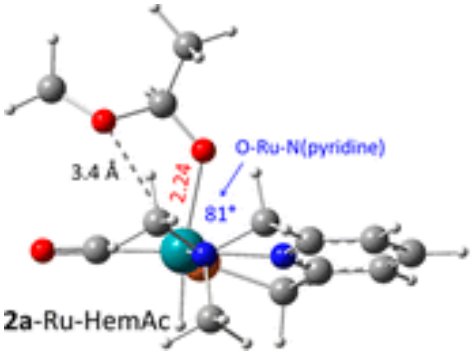


(20)

The reactions mediated by TS-Slip-2 correspond to insertion of a carbonyl group into a Ru–H bond which has ample experimental precedence. Of particular relevance to the present study are the experiments by Bergens, where cyclic esters were observed to undergo rapid insertion in *trans*-[Ru(H)$_2$(Binap)(diamine)] complexes even at low temperatures.[64] The more common examples of carbonyl insertion in octahedral complexes involve ketones [65-73] and $CO_2$.[74-80] The reverse of the insertion step in Figure 2.8 is an unconventional β-hydride elimination from an alkoxide taking place via ion-pair rearrangement without the need of a vacant coordination site, which also has experimental precedence.[81-83]

For both **3** and **4** the insertion barrier via TS-Slip-2 is slightly larger than the one for direct metathesis via TS-Slip-1. The thermodynamics of insertion on the other hand are more favored than metathesis, offering $G^{o}_{rel}$ = 5.4 or 11.4 kcal/mol for the reaction of **3** and **4**, respectively. These results imply that insertion can in practice compete with direct metathesis, but it does not provide a thermodynamics sink. However, from the insertion products it is possible to define a third ion-pair rearrangement mode via TS-Slip-3 that exchanges the coordination of the anionic C–O$^{-}$ terminal of the alkoxide with the alkoxy or the amine group. The 3-D display in eq 20 shows it should not take many structural rearrangements to reach TS-Slip-3. The latter

slippage TSs mediate aldehyde deinsertion (or elimination) from **2a**-Ru-HemAc and **2a**-Ru-HemAm. The combined insertion and deinsertion steps provide therefore an indirect ion-pair mediated route to metathesis. $G^{\ddagger}_{rel}$ of **3a**-TS-Slip-3 and **4a**-TS-Slip-3 is 16.4 and 27.5 kcal/mol, respectively, significantly smaller than the other slippage TSs. Thus, even if the kinetics were to favor insertion via TS-Slip-2 over direct metathesis via TS-Slip-1, TS-Slip-3 will still provide an energetically accessible indirect ion-pair-mediated route to metathesis.

IRC calculations starting from **3a**-TS-Slip-2 confirm a smooth connectivity between **3a**-IP-H and **2**-Ru-HemAc. IRC calculations originating in **3a**-TS-Slip-3 on the other hand lead to the insertion product **2a**-Ru-HemAc in one direction, but it converges after two steps to the same geometry as that of **3a**-TS-Slip-3. This behavior may follow from the flat nature of the PES near TS-Slip-3 which is evident from the small magnitude of the imaginary frequency in **3a**-TS-Slip-3 and **4a**-TS-Slip-3, 98i and 115i $cm^{-1}$, respectively. Animation of these vibrations leaves no doubt they are for a rotation that exchanges the coordination of the terminal O and either the OMe or NHMe group. We have located several stereoisomeric transition states of **3a**-TS-Slip-3 and **4a**-TS-Slip-3, but we could not identify any minima in the close vicinity of any of them. As shown in equation 20, TS-Slip-3 requires minimal structural arrangement of the insertion intermediate, and thus, the IRC result of a minimum near TS-Slip-3 is most likely a computational artifact.

Figure 2.9 illustrates stereospecific details pertaining to how the hemiacetaloxide or hemiaminaloxide is produced and transformed on the insertion route to metathesis.

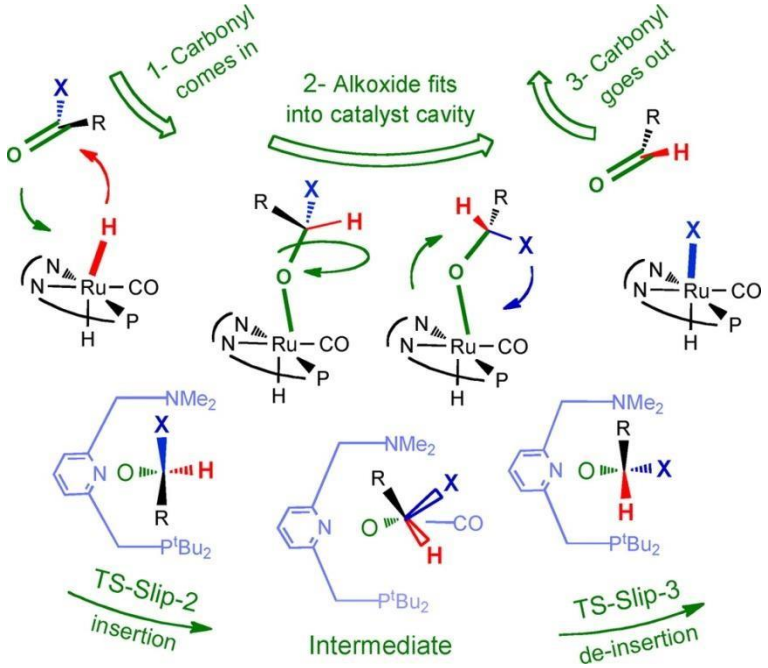


**Figure 2.9:** Stereospecific Details of the Insertion–Deinsertion Path to Metathesis

The carbonyl of **3** or **4** approaches **2**-Ru-H from the pyridine side with the alkyl group pointing toward the phosphine group. In TS-Slip-2 the exchanging C–H and C–$O^-$ bonds are aligned along the pyridine–Ru–CO axis, so the C–H bond eclipses the Ru–CO bond. As the Ru–alkoxide bond is formed, the three substituents on the tetrahedral carbon of the alkoxide are rotated so as to stagger the Ru–CO bond in between the C–H and C–X bond (X = OMe or NHMe). Continued rotation eclipses the C–X and Ru–CO bonds, providing thereby the correct alignment needed in TS-Slip-3. In the process, the orientation of the alkyl group is flipped toward the amine, and the aldehyde eliminates from the same side used in the insertion direction. Note that the alkoxide oxygen in **2a**-Ru-HemAc and **2a**-Ru-HemAm is tilted over the pyridyl ring, thus making an O–Ru–N angle of near 80° (eq 20). This structural feature appears to be common in octahedral Ru-alkoxide as was discussed elsewhere.[84]

## F. Effect of Explicit Solvent Molecule

Complete hydrogenation of **3** and **4** produces methanol. To investigate possible effects of H-bonding of the alcohol on the metathesis PESs, we conducted calculations that included a single methanol molecule to mimic an H-bond solvent donor. Starting with the separated reactants, H-bond formation between methanol and **2**-Ru-H is calculated to be slightly exoergic ($\Delta G^{o} = -1.4$ kcal/mol) so we take this species as the reference point in defining the energies of the other points on the PESs. For each ion-pair the methanol was introduced such that it undergoes an H-bond with the formally "anionic" oxygen center. The results summarized in Figure 2.10 show the methanol molecule stabilizes all of the ion-pair TSs in the reaction of both **3** and **4** by 3–5 kcal/mol. The effect is not unexpected, since the given reactions replace an H-bond between methanol and a metal-hydride in the reactants by a stronger H-bond involving a negatively charged oxygen in the ion-pair minima and TSs.

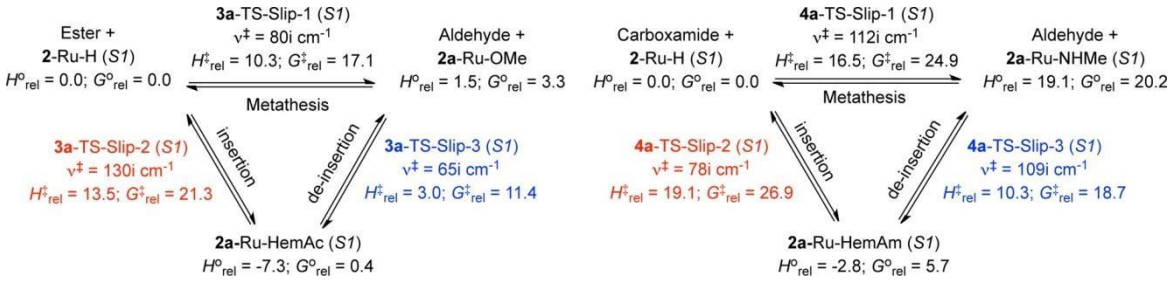


**Figure 2.10.** Energies of the slippage TSs computed while including a methanol molecule (*S1*) to mimic an explicit H-bond donor solvent. Free energies are given in kcal/mol relative to the methanol-solvated **2**-Ru-H and either **3** or **4**.

## G. Indirect metathesis via MLC

In this section we examine more closely the metal–ligand cooperative (MLC) route to hydrogenation. For this purpose Figure 2.11 tracks an outer-sphere PES that

allows interaction between the carbonyl oxygen of **3** or **4** with the axial proton of the phosphine arm of **2**-Ru-H (distinguished as path **b**; see eq 13).

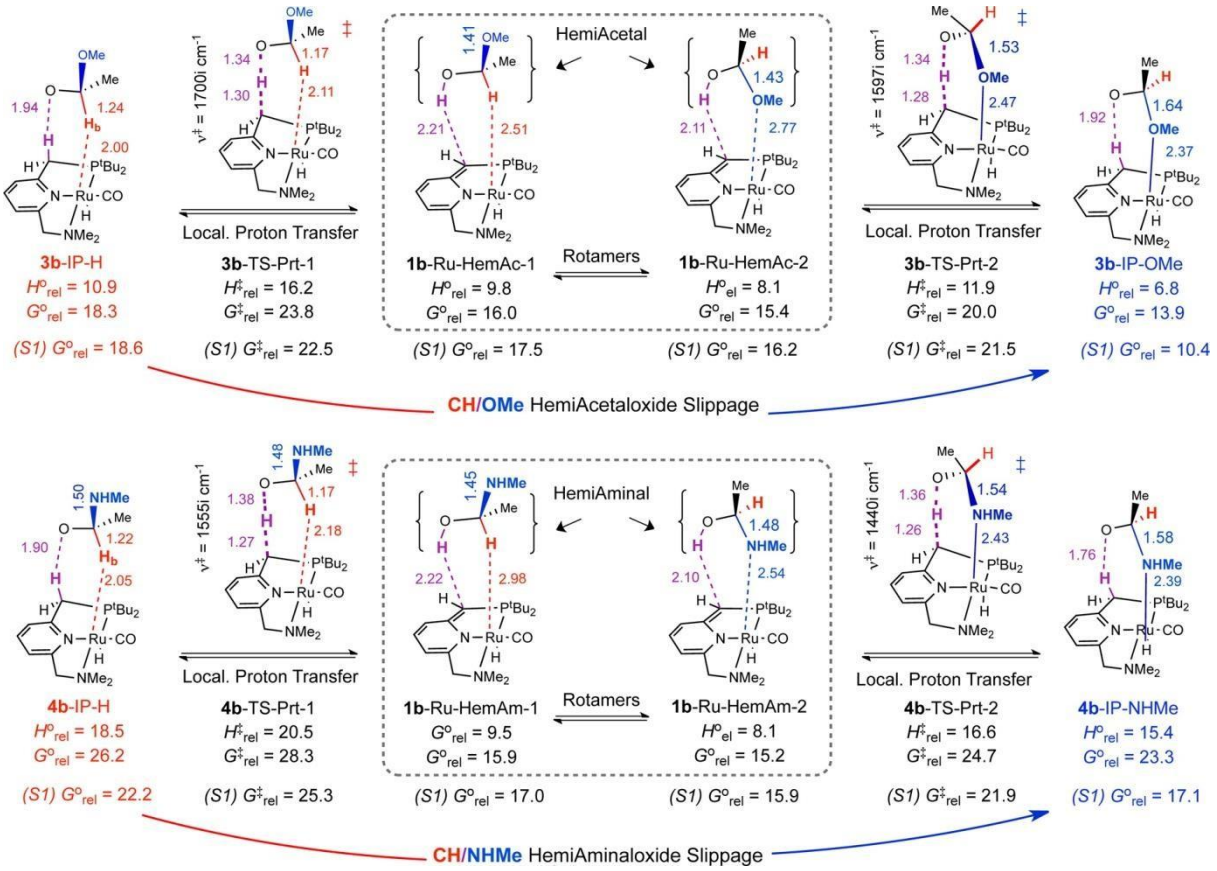


**Figure 2.11.** Reaction between **2**-Ru-H and **3** or **4** on path **b** involving ligand deprotonation. The energies are given relative to the separated reactants in kcal/mol.

As found in Figure 2.1, hydride transfer from **2**-Ru-H to methyl acetate on path **b** yields a C–H ion-pair minimum (**3b**-IP-H), but this time the terminal oxygen of the hemiacetaloxide is pointed at the axial C–H proton of the phosphine arm at a distance of 1.94 Å. From **3b**-IP-H, proton transfer from the PNN ligand to the terminal oxygen of the hemiacetaloxide via **3b**-TS-Prt-1 has a barrier of 5.5 kcal/mol. The immediate product from this step is **1b**-Ru-HemAc-1, a loose precomplex between a hemiacetal and the neutral square pyramidal **1**-Ru in which the C–H bond of the hemiacetal is pointed to the metal at a distance of 2.5 Å and the alcoholic proton is at 2.2 Å from the

deprotonated carbon of the phosphine arm. $G^{‡}_{rel}$ of **3b**-TS-Prt-1 is 23.8 kcal/mol (in toluene), slightly higher than the energy of **3a**-TS-Slip-1 in Figure 2.1 (21.8 kcal/mol). Thus, in spite of the very different character of the two reactions, the slippage and ligand deprotonation TSs appear to be competitive. However, for hydrogenation to proceed, the hemiacetal produced after proton transfer would still need to undergo further hydrogenolysis of the C–OR bond. In investigating a possible role of **1**-Ru in the latter reaction we considered the MLC mechanism reported in the study by Wang.[39] This led us to identify **3b**-TS-Prt-2 in Figure 2.11 having $G^{‡}_{rel}$ = 20.0 kcal/mol. We find the geometry (near linear C–H–O angle), imaginary frequency (1600i $cm^{-1}$), reduced mass (1.1 amu), and the animation of the imaginary frequency of **3b**-TS-Prt-2 to be all fully characteristic of a localized motion of the alcoholic proton between an OMe-coordinated hemiacetal precomplex and the carbon of the phosphine arm. This differs from the delocalized description of the same TS in which the C–OR bond is cleaved concomitantly with proton transfer.[39] Consistent with a localized proton transfer step, Figure 2.11 shows **3b**-TS-Prt-2 to connect an OMe-coordinated conformer of a hemiacetal precomplex of **1**-Ru (**1b**-Ru-HemAc-2) with an OMe-coordinated hemiacetaloxide ion-pair (**3b**-IP-OMe). This means that the combined MLC sequence of hemiacetal formation and subsequent reaction with **1**-Ru simply switches the C–H coordination of the hemiacetaloxide produced right after hydride transfer into the more favorable mode in which the OMe group points to the metal. In other words the given deprotonation and protonation sequence of the ligand provides an indirect route to interchanging the C–H and C–OMe ion-pairs taking place on path **b**. Further cleavage of the C–OMe bond from **3b**-IP-OMe will complete an MLC-mediated H/OR metathesis. The same is true for the sequence involving the reaction of the carboxamide

in Figure 2.11, where a hemiaminal is formed by ligand deprotonation via **4b**-TS-Prt-1, rotated to bind the amine to the metal in **1b**-Ru-HemAm-2, and then deprotonated via **4b**-TS-Prt-2 to give the amine-coordinated hemiaminaloxide ion-pair (**4b**-IP-NHMe). The latter ion-pair still needs to undergo aldehyde elimination to complete a metathesis. As discussed in Figure 2.4, C–NHMe bond cleavage starting from **4b**-IP-NHMe proceeds by a distinct TS (**4b**-TS-NHMe) with $G^{\ddagger}_{rel}$ = 26.4 kcal/mol.

IRC calculations confirm the connectivities associated with a localized proton transfer originating from the C–H bound **3b**-TS-Prt-1 and **4b**-TS-Prt-1. Likewise, for the NHMe-bound deprotonation of the hemiaminal by **1**-Ru, the IRC starting from **4b**-TS-Prt-2 converges into the expected hemiaminal precomplex in one direction and the NHMe-bound ion-pair of the hemiaminaloxide in the other (blue line in Figure 2.12).

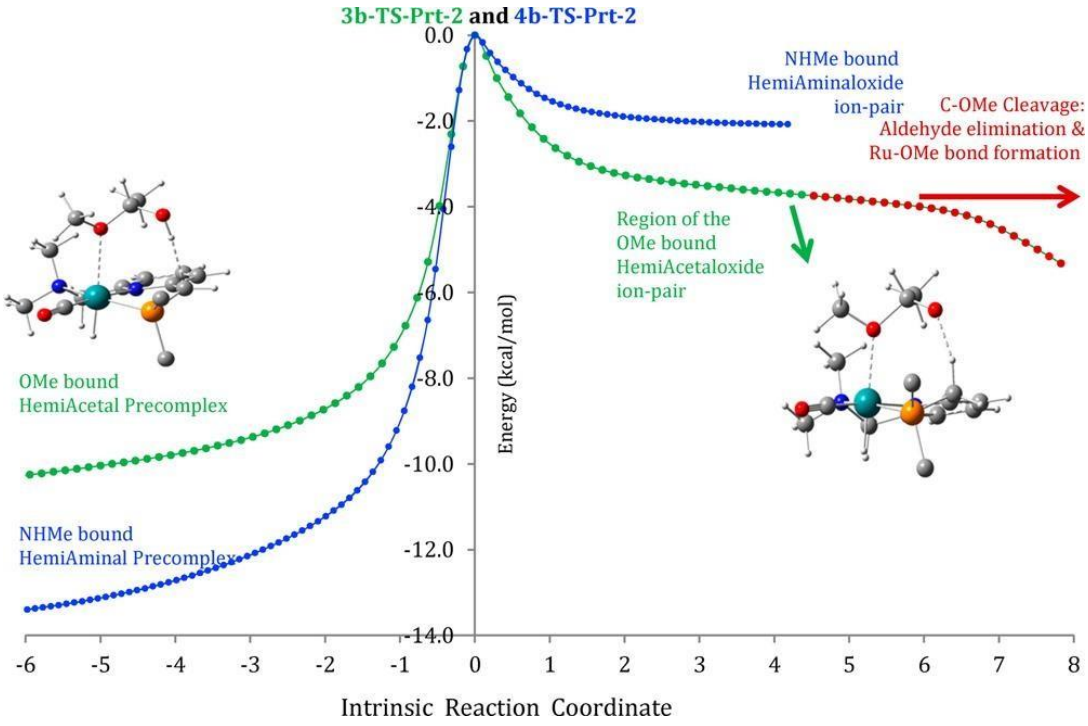


**Figure 2.12**. Intrinsic reaction coordinates originating from **3b**-TS-Prt-2 (hemiacetal; green curve) and **4b**-TS-Prt-2 (hemiaminal; blue curve). M06 gas phase electronic energies defined relative to the TSs in kcal/mol.

For the reaction of the OMe-bound hemiacetal on the other hand, the IRC originating from **3b**-**TS**-Prt-2 converges to the OMe bound hemiacetal precomplex in one direction, but it reaches a plateau in the direction of the OMe bound ion-pair and then proceeds with elimination of the aldehyde (Figure 2.12). This result enforces the proposition that once the OMe group of the hemiacetaloxide anion gets in the vicinity of the metal there will be no barrier to C–OMe cleavage and Ru-alkoxide formation. In spite of the lack of a distinct TS for C–OMe cleavage, the IRC from **3b**-TS-Prt-2 in Figure 2.12 is still most consistent with a dehydrogenation mechanism of the hemiacetaloxide in which the proton is transferred separately from C–OMe cleavage. We emphasize that the calculations do identify a true minimum for the OMe-bound hemiacetaloxide ion-pair on path **b** (**3b**-IP-OMe in Figure 2.11). This minimum is very shallow, and we argue it is best viewed as an activated species on the PES that undergoes a barrierless C–OR bond cleavage. To some extent therefore, the **3a**-TS-Slip-1 is effectively like a concerted metathesis TS.

## H. Energy of the Slippage and MLC TSs

Table 2 compares the energies of the slippage and the C–H-bound proton transfer TSs in the reactions of **3** and **4** using different density functionals and solvent continuums. For the ester, the M06L $G^{\ddagger}_{rel}$ of **3b**-TS-Prt-1 in toluene (23.8 kcal/mol) is slightly higher than **3a**-TS-Slip-1 (21.8 kcal/mol). For *N*-methylacetamide on the other hand, the M06L $G^{\ddagger}_{rel}$ of **4b**-TS-Prt-1 is 28.3 kcal/mol, 1.9 kcal/mol *lower* than $G^{\ddagger}_{rel}$ of **4a**-TS-Slip-1 (30.2 kcal/mol; in toluene continuum). The ωB97X-D or the M06L levels selectively stabilizes the proton transfer TSs (to 24.2 kcal/mol), thus increasing the preference for **4b**-TS-Prt-1 over **4a**-TS-Slip-1 to 4.6 kcal/mol (in toluene; Table 2). The

results are not changed when full geometry minimization and normal-mode analysis are done at the ωB97X-D level.

| | ester reactions | | carboxamide reactions | |
|---|---|---|---|---|
| | **3a-TS-Slip-1** | **3b-TS-Prt-1** | **4a-TS-Slip-1** | **4b-TS-Prt-1** |
| **M06 (toluene)[a]** | 16.9 | 21.8 | 30.0 | 26.2 |
| **M06L (toluene)[a]** | **21.8** | **23.8** | **30.2** | **28.3** |
| **ωB97X-D (toluene)[a]** | 20.9 | 20.4 | 29.6 | 24.2 |
| **M06L (THF)[a]** | 23.6 | 26.3 | 31.8 | 31.5 |
| **M06L (methanol)[a]** | 14.8 | 24.2 | 28.2 | 30.9 |
| **Opt M06-L (Tol)[b]** | 21.6 | 23.3 | 30.0 | 27.6 |
| **Opt ωB97X-D (Tol)[c]** | 20.8 | 21.3 | 29.9 | 24.7 |
| **(*S1*) M06L (Tol)[a]** | 17.7 | 19.5 | 24.9 | 25.3 |

**Table 2.** $G^{\ddagger}_{rel}$ of TS-Slip-1 and TS-Prt-1 at Different Theoretical Levels (in kcal/mol)

a Results from single-point calculations on geometries minimized in the gas phase at the M06 level.
b Geometries and frequencies computed in the gas phase at the M06L level.
c Geometries and frequencies computed in the gas phase at the ωB97X-D level.

The computed reversal in the energy order of the direct slippage and ligand deprotonation TSs in the reaction of the carboxamide compared to the reaction of the ester follows in part from a significantly larger proton affinity of the hemiaminaloxide anion compared to the hemiacetaloxide ($\Delta\Delta G^{o}$ = −6.4 kcal/mol; eq 21; favoring proton transfer in the reaction of **4**), and in part from a slightly larger barrier for rearrangement from IP-H to TS-Slip-1 in the carboxamide case ($\Delta\Delta G^{\ddagger}$ = 1.4 kcal/mol; Figure 2.1; disfavoring slippage in the reaction of **4**).

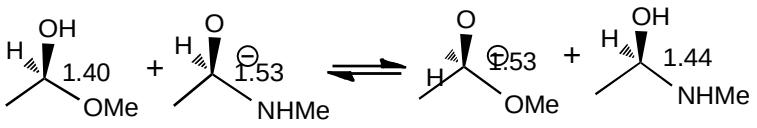

(21)

Given the ion-pair and acid–base nature of the given transformations, the precise contribution of the two paths to metathesis is expected to depend on dynamics

and solvent effects details.[85] Such effects can be different for the two routes, but they are difficult to compute accurately. Thus, when a THF solvent continuum is used in the calculations, the M06L energies of **4a**-TS-Slip-1 and **4a**-TS-Prt-1 become nearly identical (Table 2), and in a methanol continuum the slippage TS becomes lower than the proton transfer TS by 2.7 kcal/mol. Furthermore, when a methanol molecule is included as an explicit H-bond donor in the calculations, the M06L **4a**-TS-Slip-1 becomes 0.4 kcal/mol *lower* than **4b**-TS-Prt-1 even in the toluene continuum (*S1* entries in Figures 2.10 and 2.11). We stress that the two TSs being compared are on two PESs leading to the same OR- or NHR-bound hemiacetaloxide and hemiaminaloxide ion-pairs, which we propose to activate the C–OR and C–NHR bonds in preparation for aldehyde elimination to complete an H/OR or H/NHR metathesis. In fact at the ωB97X-D level the barrier to C–NHMe cleavage on the MLC path via **4b**-TS-NHMe discussed in Figure 2.4 is 29.6 kcal/mol, significantly higher than that via **4b**-TS-Prt-1 (24.2 kcal/mol) and identical to that via **4a**-TS-Slip-1. The OR- and NHR-bound ion-pairs were not identified in previous computational studies of the MLC mechanisms. Consideration of these ion-pairs gives a fundamentally new perspective to understanding the metal-catalyzed C–OR and C–NHR bond cleavage step in the reaction of **2**-Ru-H with **3** and **4** regardless of how the IPs are formed. In addition to the slippage and MLC rearrangement modes, one can envision other routes to obtain the OR and NHR ion-pairs, such as by full dissociation and reassociation of the ion-pairs, formation of solvent separated ion-pairs, or by a protonation and deprotonation sequence of the anion by the alcohol that is produced during hydrogenation. Again, the contribution of such routes will depend on solvent and dynamics effects that may vary as the concentration of the alcohol is changed during the course of catalytic

hydrogenation. The reaction via TS-Slip-1 provides sort of the least action path to rearrange the ion-pairs. The data in Table 2 shows this path to be at least competitive with the MLC mechanism involving ligand deprotonation and reprotonation.

## I. Metathesis in the Dehydrogenative Coupling Direction

In this section we discuss the ion-pair PESs in the context of amine dehydrogenative coupling. To be able to address the question of the observed selectivity to carboxamides using the same data for methyl acetate and *N*-methylacetamide hydrogenation, we start with **1**-Ru in a mixture of ethanol, methanol, and methylamine. The computed free energy of ethanol addition to **1**-Ru is −6.9 kcal/mol, compared to −5.0 and +6.8 kcal/mol for methanol and methylamine addition, respectively. According to these results the resting state of the catalyst in the given mixture should be the octahedral ruthenium–ethanoxide (**2a**-Ru-OEt), so we place this complex along with methanol and methylamine at the zero level on the Gibbs free energy scale in Figure 2.13).

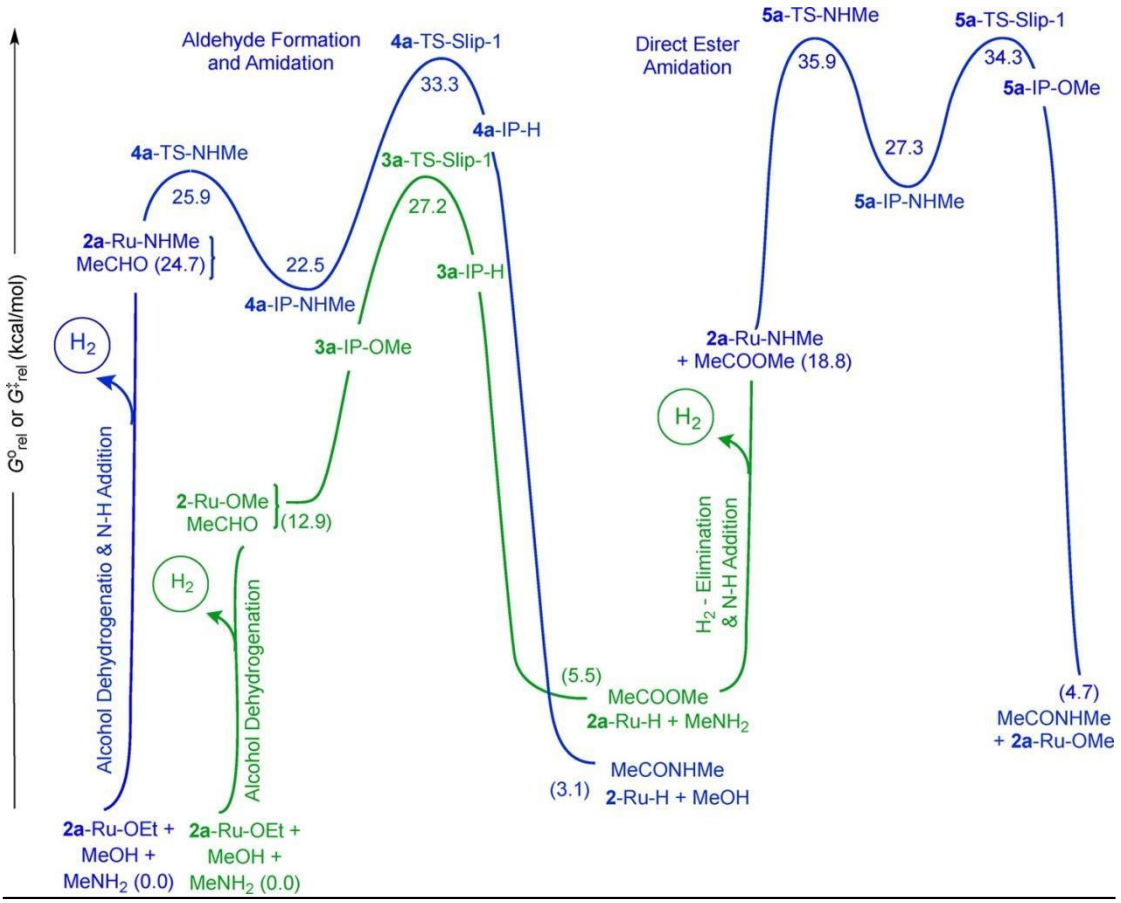


**Figure 2.13.** Standard state Gibbs free energy profiles (298 K; 1 atm) for dehydrogenative coupling starting with **1**-Ru in a mixture of methanol, ethanol and methylamine (M06L-toluene; in kcal/mol)

To produce methyl acetate from the given mixture, the mechanism under consideration requires a preparatory stage in which **2a**-Ru-OEt is dehydrogenated into acetaldehyde and $H_2$ along with the formation of **2**-Ru-OMe. The thermodynamics of this stage is uphill by 12.9 kcal/mol. Again, for our purposes we can ignore the barriers in the preparatory stage. Coupling between the aldehyde and **2a**-Ru-OMe to give the C–OMe-bound hemiacetaloxide ion-pair is exothermic by 1.1 kcal/mol, but because of the unfavorable entropy term, the step is uphill by 6.0 kcal/mol (Figure 2.1), so $G^{o}_{rel}$ of **3a**-IP-OMe in Figure 2.13 is 19.5 kcal/mol. To eliminate an ester, the hemiacetaloxide must rearrange to orient the C–H bond toward the metal. The rearrangement barrier

from the shallow **3a**-IP-OMe via **3a**-TS-Slip-1 is 8.3 kcal/mol. **3a**-TS-Slip-1 is the highest energy point on the given PES, with a $G^{\ddagger}_{rel}$ value of 27.2 kcal/mol. The thermodynamics for transformation from the initial reactants into **2**-Ru-H and the ester is uphill by 5.5 kcal/mol.

To form *N*-methylacetamide from the initial mixture in Figure 2.13, the preparatory stage requires dehydrogenation of **2a**-Ru-OEt as well as reaction of the amine to give **2a**-Ru-NHMe. Because the thermodynamics of amine addition to **1**-Ru is unfavorable (Table 1), the energy input for this stage is large: 24.7 kcal/mol. Coupling of aldehyde with **2a**-Ru-NHMe into **4a**-IP-NHMe encounters a small barrier estimated at 1.2 kcal/mol in Figure 2.1, but opposite to the reaction of **2a**-Ru-OMe, the coupling involving C–N bond formation is *exoergic* by 2.1 kcal/mol. However, the slippage barrier of the hemiaminaloxide needed to reach the C–H ion-pair is substantial (10.7 kcal/mol), so **4a**-TS-Slip-1 comes to 33.3 kcal/mol on the PES. The combined results indicate strongly therefore that, at least for the given substrates, dehydrogenative coupling into an ester should be kinetically much more favored than coupling into a carboxamide ($\Delta\Delta G^{\ddagger}_{rel}$ = 6.1 kcal/mol). When the respective MLC routes are considered, the highest energy points on the two coupling PESs will be **3b**-TS-Prt-1 and **4b**-TS-Prt-1 with $G^{\ddagger}_{rel}$ = 29.2 and 31.4 kcal/mol, respectively, still in favor of ester formation. Note that **4a**-IP-H in Figure 2.13 is 4.6 kcal/mol above **3a**-IP-H. These C–H ion-pairs are effectively the TSs for the final hydride transfer steps needed to eliminate the carboxamide or the ester. As such, it is unlikely there can be other metal-catalyzed mechanisms to coupling involving aldehydes that would selectively favor the population of the higher energy **4a**-IP-H to give a carboxamide as a kinetic product.

The computed kinetic preference to the ester in Figure 2.13 is opposite to the experimentally observed selectivity to carboxamides. However, the carboxamide is the thermodynamically favored product in the Figure ($\Delta\Delta G^{o}_{rel}$ = −2.4 kcal/mol). It is possible, therefore, that the ester can in practice be formed as a kinetic product, but it gets amidated under the experimental conditions, a possibility that had been raised in the studies by Milstein. As mentioned in the Introduction, complexes related to **1**-Ru are indeed known to catalyze ester amidation (eq 4), an interesting and valuable reaction in its own.[25, 26]

Ester amidation under the alcohol-amine coupling conditions can in principle proceed on the same PESs involving the aldehyde. This will require the ester and **2**-Ru-H products to revert back to acetaldehyde and **2a**-Ru-OMe so the acetaldehyde may react with **2a**-Ru-NHMe to form the thermodynamically more favored carboxamide. In Figure 2.14 we give evidence for the accessibility of an alternative ion-pair NHR/OR metathesis route that achieves ester amidation in a more direct way.

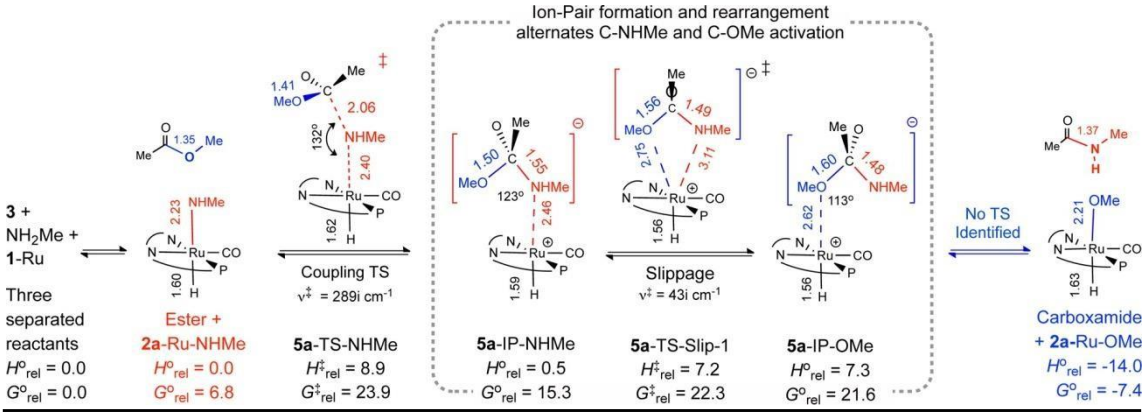


**Figure 2.14.** Stationary points on the outer-sphere PES in the reaction of an ester (**3**) and **2**-Ru-NHMe. Energies are given in kcal/mol relative to the separated reactants (M06L-toluene).

## J. Ester Amidation via NHR/OR Metathesis

The energies in Figure 2.14 are defined relative to the separated square pyramidal **1**-Ru, methylamine and methyl acetate, thus mimicking the initial conditions of an ester amidation experiment utilizing an alkyl amine. From this mixture the preparatory stage for an NHR/OR metathesis of the ester involves only methylamine addition to **1**-Ru, so the required energy input is relatively small, 6.8 kcal/mol. Coupling between the ester and **2**-Ru-NHMe gives an amine-coordinated ion-pair minimum of the α,α-(NHMe)(OMe)-ethanoxide anion (**5a**-IP-NHMe). The thermodynamics of the coupling step is computed to be nearly thermoneutral ($\Delta H^{o}_{Add}$ = 0.5 kcal/mol), affording $\Delta G^{o}_{Add}$ = 8.5 kcal/mol, but the step has a relatively high barrier via **5a**-TS-NHMe with $\Delta H^{\ddagger}_{Add}$ and $\Delta G^{\ddagger}_{Add}$ of 8.9 and 17.1 kcal/mol, respectively. **5a**-TS-NHMe is characterized by a C–N bond distance of 2.06 Å and $\nu^{\ddagger}$ = 289i $cm^{-1}$ for C–N stretching vibration. Subsequent slippage via **5a**-TS-Slip-1 in Figure 2.14 rearranges the α,α-(NHMe)(OMe)-ethanoxide within the intact ion-pair to coordinate the methoxy group to the metal (**5a**-IP-OMe). The switch from NHMe to OMe coordination causes a contraction in the C–NHMe bond from 1.55 to 1.48 Å, and a stretch in the C–OMe bond from 1.50 to 1.60 Å, demonstrating again that metal-coordination activates the respective bonds. From **5a**-IP-OMe, cleavage of the C–OMe bond into **2a**-Ru-OMe and *N*-methylacetamide is highly exoergic ($\Delta G^{o}_{Diss}$ = −29.7 kcal/mol), and a PES scan reveals the reaction to be totally barrierless. The net transformation in Figure 2.14 is an ion-pair-mediated metathesis in which an amide and alkoxide are exchanged between a ruthenium amide and an ester. Unlike the metatheses involving H/OR, H/NHR (Figure 2.1) or OR/OR exchange,[55] the highest energy point on the NHMe/OMe metathesis PES in Figure 2.14 is for the TS of the ester–amide coupling step, and not the slippage

TS. The difference between the two TSs is however small (23.9 vs 22.3 kcal/mol). Thus, ester amidation is highly exoergic, and the direct metal-mediated metathesis route provides a surprisingly low energy barrier for the transformation.

In studying ester amidation, we also considered the MLC route to an NHR/OR ion-pair rearrangement. The transition state for ligand deprotonation on path **b** via the NHMe-coordinated α,α-(NHMe)(OMe)-ethanoxide (**5b**-TS-Prt-1; eq 22) has $G^{o}_{rel}$ = 22.6 kcal/mol, similar to **5a-TS**-Slip-1 (22.3 kcal/mol; M06L-toluene). However, the TS for ligand reprotonation via the OMe-coordinated anion (**5b**-TS-Prt-2; eq 22) is 26.3 kcal/mol, indicating the MLC route is overall less favored than ion-pair slippage.

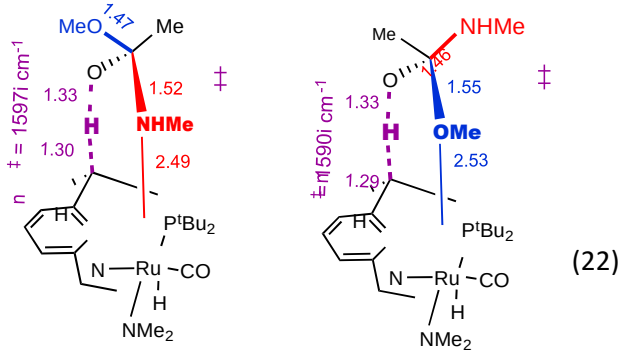


(22)

**5b**-TS-Prt-1 $H^{‡}_{rel}$ = 7.0; $G^{‡}_{rel}$ = 22.6

**5b**-TS-Prt-2 $H^{‡}_{rel}$ = 11.3; $G^{‡}_{rel}$ = 26.3

When considered in the context of amine-alcohol coupling discussed in Figure 2.13, ester amidation has to start from **2**-Ru-H, the ester, and the free amine. The energy of the latter species on the scale in Figure 2.13 is 5.5 kcal/mol. The preparatory stage for ester amidation requires $H_2$ elimination and **2**-Ru-NHMe formation, with an energy input of 13.4 kcal/mol. This puts **5a**-TS-NHMe and **5a**-TS-Slip-1 at 35.9 and 34.4 kcal/mol, slightly higher than **4a-TS**-Slip-1 (33.3 kcal/mol) for ester amidation via the (reversible) aldehyde route. However, the energy scale in Figure 2.13 applies to a condition where each species, including $H_2$, is present under standard state conditions (1

atm and 298 K). Experimentally, coupling is possible only because $H_2$ is liberated from the reaction mixture under reflux, so taking the energy of the "final" ester product as +5.5 kcal/mol on the amidation NHR/OR PES in Figure 2.13 is clearly not representative of the catalytic system, and the contribution of the direct NHR/OR route may in practice be much greater than the one suggested by the standard state energy profile. To put it differently, because $H_2$ is removed from the reaction mixture under dehydrogenative coupling conditions, rehydrogenolysis of the ester into an aldehyde and an alcohol becomes less likely, leaving the ester/amine coupling route as the "only" remaining option for carboxamide formation. Interestingly, if esters are produced and amidated in the dehydrogenative coupling of amines into carboxamides, esters can in turn be produced and hydrogenated in the reverse *hydrogenation* of carboxamides starting with **2**-Ru-H. This most unusual inference should of course be valid independent of the true mechanism of ester amidation. In the ion-pair slippage framework, carboxamide hydrogenation would initially proceed by the H/NHR metathesis route described in Figure 2.1. As the reaction proceeds, the concentration of the alcohol will increase. If the equilibrium concentration of **2a**-Ru-OR under $H_2$ becomes significant, it can undergo an OR/NHR metathesis with the carboxamide to give an ester and **2a**-Ru-NHR. **2a**-Ru-NHR will give the amine hydrogenation product. Figure 2.1 establishes that hydrogenation of the ester using **2**-Ru-H should be comparatively fast, so this will give the second hydrogenation (alcohol) product of the initial carboxamide.

## K. Conclusion

Based on detailed electronic structure calculations, the present study proposes that the dehydrogenative coupling of amines with alcohols or esters into carboxamides that can be catalyzed by Milstein's $d^6$-[Ru(PNN)(CO)(H)] catalysts (**1**-Ru) can be understood in terms of simple metal/acyl metathesis transformations. The study assumes that alcohol dehydrogenation into aldehydes is an accessible transformation in the given systems. We start with the observation that complexes related to **1**-Ru undergo characteristic metal–ligand cooperative (heterolytic) addition of $H_2$, ROH and $NH_2R$ to give octahedral $d^6$-ruthenium complexes (**2**-Ru-X) in which a hydride, alkoxide, or an amide is positioned trans to a hydride (Figure 2.16).

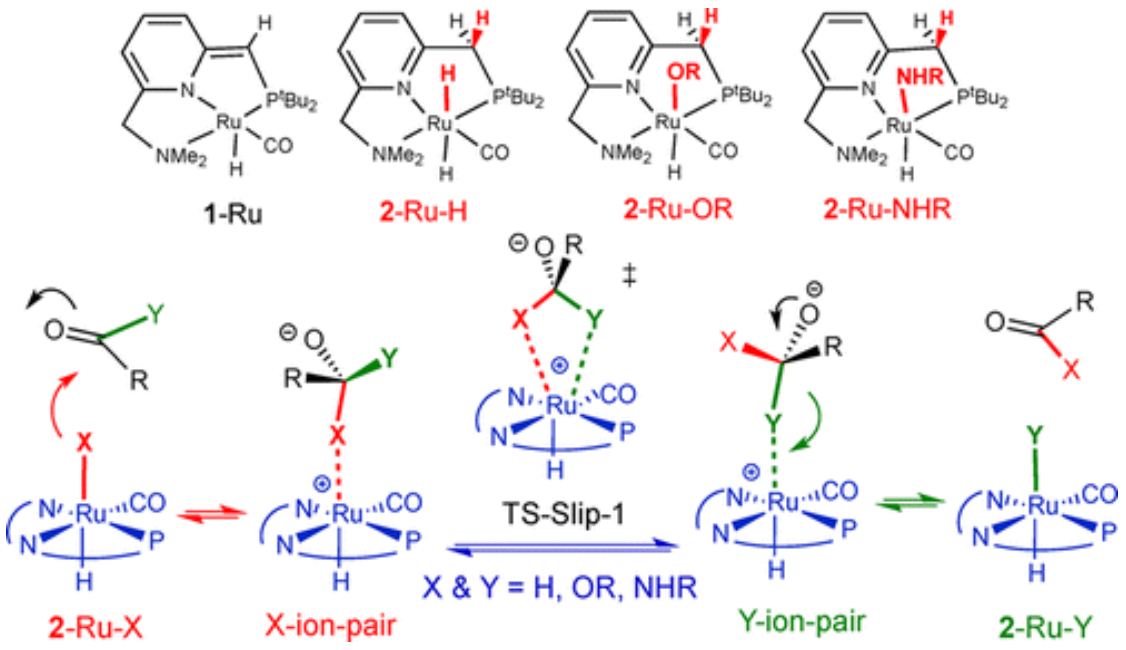


**Figure 2.16**. X/Y - metal/acyl metathesis

Hydride transfer from a metal complex such as **2**-Ru-H to a carbonyl group is familiar. Our idea is that the coordinated alkoxide and amide anions ($X^-$) of the other octahedral complexes can undergo similar reactions with an aldehyde or an ester

(RCYO). The immediate product from such reactions on the PES is an uphill contact ion-pair of an α-substituted alkoxide anion ($RCXYO^-$) in which the newly formed C–X bond is coordinated to the metal (X-ion-pair). The coordination of the X group appears to activate the corresponding C–X bond. At first there appears to be nothing unusual or remarkable about the given "transfer" or "coupling" steps. However, if we accept that X can move from **2**-Ru-X to an organic acyl-Y molecule, it becomes evident that the same reaction can take place in reverse from the α-substituted alkoxide via Y. This produces a new octahedral ruthenium complex (**2**-Ru-Y) and a new organic acyl-X product. The net reaction is a novel metathesis in which X and Y are interchanged between a metal and an acyl group. This simple reaction can be readily used to rationalize much of Milstein's extraordinary chemistry. All is needed here is a trivial rotation of the α,α-(X)(Y)-substituted alkoxide to orient Y in the direction of the metal. The calculations show the process can take place in a least action mode via TS-Slip-1. The characterization of the individual X or Y transfer regions on the PES proved to be a tedious exercise in locating shallow ion-pair minima and elusive flat TSs that can easily be absent from the PES. At the end, the results reveal the H/OR and H/HNR slippage TSs to be the highest energy point on the metathesis PES. For these cases the full metathesis PES is in effect like a single concerted step taking place via TS-Slip-1. For the NHR/OR metathesis on the other hand, the highest energy point is the TS for C–N coupling between the ester and metal-coordinated amide, but this is only slightly higher than the slippage TS. If it occurs without a barrier, ion-pair dissociation into free ions and reassociation by a different group would provide a variation to the ion-pair rearrangement mechanism that would circumvent the slippage TS.

The present study shows that the hydrogenation MLC mechanism involving hemiacetal and hemiaminal formation followed by a metal mediated fragmentation is simply an indirect multistep route to the same metathesis that can be mediated by ion-pair rearrangement. The MLC and ion-pair slippage routes to metathesis are computed to be competitive. A definitive theoretical comparison of the possible role of the different routes to the same reaction in catalysis requires dynamics effects and accurate estimates of both the basicity of the α-substituted alkoxides and solvation of the ion-pair, which are not easy to evaluate computationally. We demonstrate for example that changing the solvent continuum from toluene to THF or methanol, or including a methanol molecule explicitly in the calculations shift the results in favor of the ion-pair slippage route. These computed results cannot rule out a role for MLC in catalysis, but at the same time they do indicate that the more direct slippage route is also plausible. Taken at face value, our results based on conventional transition state theory and implicit bulk treatment of solvation indicate that the dehydrogenative coupling of methyl amines with ethanol using **1**-Ru proceeds by initial formation of an ester via an ion-pair OR/H metathesis followed by ester amidation via a low energy ion-pair NHR/OR metathesis.

# CHAPTER III

# DIRECT METATHESIS FOR HYDROGENATION OF ESTERS WITH POTENTIAL CATALYSTS

## A. Overview

The MLC and ion-pair mediated mechanisms provide fundamentally different routes to achieve the same H/OR metathesis reaction. As stated in the conclusion, given the very different nature of the elementary reactions on the two pathways, the computed small preference for the ion-pair mediated pathway cannot rule out a role of MLC in catalysis. As such it becomes of interest to be able to identify possible experiments that may distinguish between the two. One such possibility is to identify target compounds that would lack the acidic proton. However, the methylene linker can in fact exert structural or electronic effects that facilitate the kinetics of the H/OR metathesis in one way or another. The calculations can be particularly useful in comparing the reactivity of related complexes.

In this section we consider two analogs of 1-Ru-H that lack a methylene unit of the phosphine arm namely $1^{CF2}$-Ru-H and $1^{O}$-Ru-H.

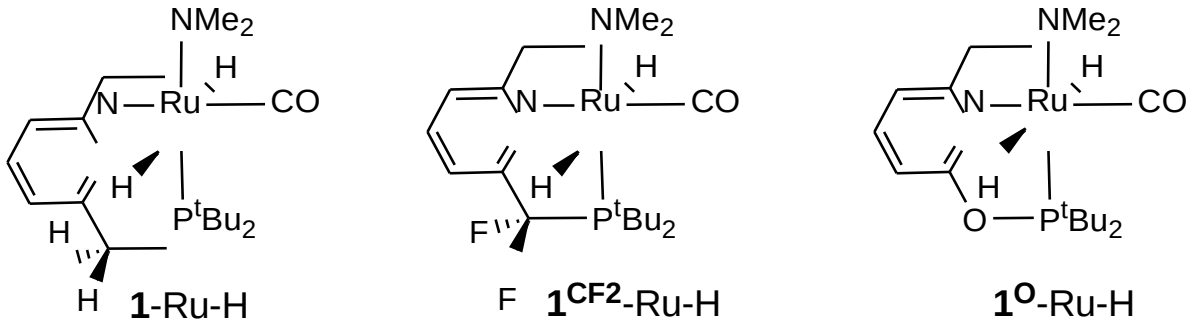


**Figure 3.1**: Milstein's octahedral catalyst (left), and after replacing the $CH_2$ linker by $CF_2$ (center) and by O (right).

**1**$^{CF2}$-Ru-H gets rid of the acidic protons in **1**-Ru-H by simply substituting the tetrahedral methylene linker of the phosphine arm by another tetrahedral $CF_2$ one. **1**$^{O}$-Ru-H on the other hand, substitutes the $CH_2$ linker by an oxygen atom. As shown in the following figure and Table, the optimized geometries of the two complexes have significant differences. Taking the dihedral angle to be measured between the phosphorous, the two carbons of the methylinic linkers and the nitrogen, values of the angles for **1**-Ru-H and **1**$^{CF2}$-RuH are around 48$^{o}$. Upon substitution of the linker by oxygen, the degree of tilting is decreased to 38. The change in the dihedral changes the spacing over the catalyst where slippage takes place.

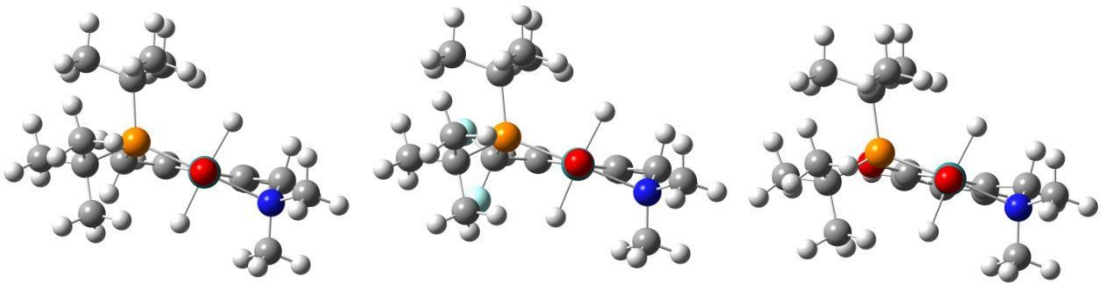

| Octahedral Complex | Dihedral Angle (degree) |
|---|---|
| **1-Ru-H** | **47.6** |
| **1$^{CF2}$-Ru-H** | **47.7** |
| **1$^{O}$-Ru-H** | **38.4** |

**Figure 3.2:** 3-D side view of 1-Ru-H (left), 1$^{CF2}$-Ru-H (center), and 1$^{O}$-Ru-H (right) along with their corresponding dihedral angles.

## B. Ester Hydrogenation with $1^{CF2}$-Ru-H

We follow the same approach as the main reaction pathway that has been discussed in the previous chapter, taking the simplest ester, methyl acetate, as the reference for calculations.

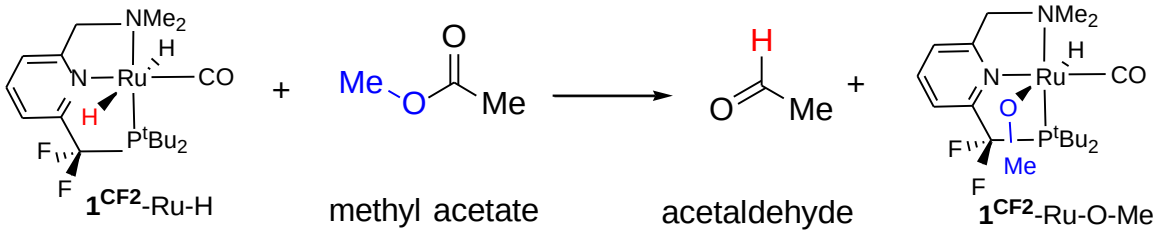


We compare the results of the potential catalyst ($1^{CF2}$-Ru-H) with the one previously calculated (1-Ru-H), under the same levels of theory that was used in the previous chapter; we find out that the energy values are comparable. In the previous 1-Ru-H reported data, the reaction path with the most thermodynamically favored conditions were found to be using toluene as a solvent and under the M06L basis set in SMD continuum.

First of all, comparing the two catalysts, 1-Ru-H and $1^{CF2}$-Ru-H, we can find out that for the reported data for the Ru-H bond lengths are 1.73 and 1.71 Angstrom respectively while the hydrides in the $1^{CF2}$-Ru-H are of bond lengths 1.74 and 1.70 Angstroms respectively; this could be an indicator of relatively different activations of the trans hydrides of the potential catalyst as well as the original 1-Ru-H catalyst. In addition, both complexes exhibit a puckered octahedral geometry; a factor that would certainly enhance exposing the hydride to the carbonyl.

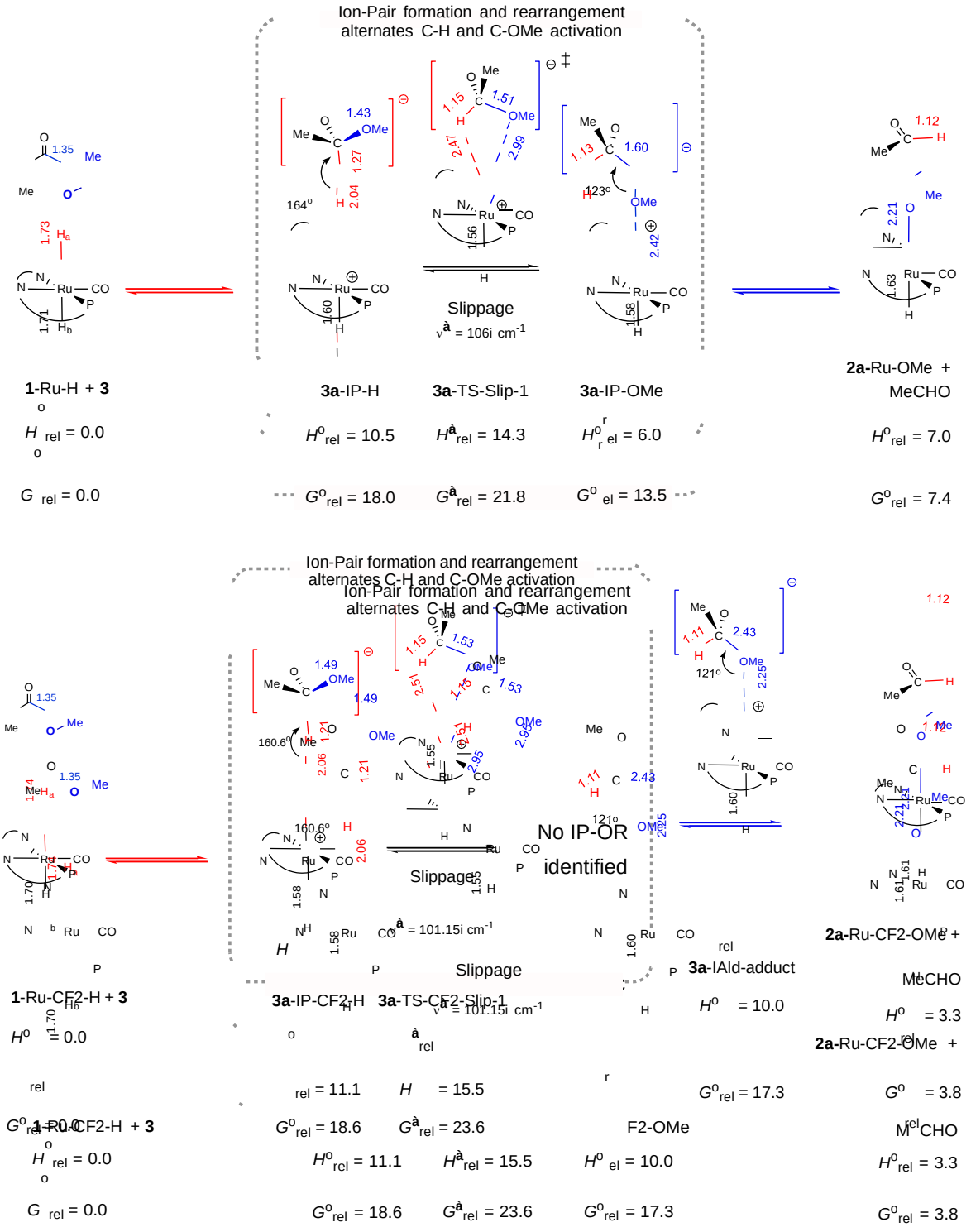


**Figure 3.3:** Comparison of the potential energy surfaces of the catalysis of 1-Ru-H (top) and 1-Ru-CF2-H (bottom) under M06 level using toluene as a solvent.

In both cases mentioned, the reaction under study can be broken down into two consecutive parts, the hydride transfer from the Ruthenium to the carbonyl which will

result in a positively charged metal complex and a negatively charged carbonyl. The second step involves the transfer of the Alkoxide from the carbonyl to the Ruthenium center of the catalyst ending up with an alkoxy group coordinated with the metal and an aldehyde. Those two steps are mediated by a transition state that is thought of to be as a rotation of the carbonyl bond where the hydride, originally pointing at the metal center, would exchange positions with the alkoxide, rendering the oxygen pointing to

Ruthenium. In addition, the focus in this part of the study is to compare the energies of the slippage mechanism, for this reason, the focus was only on the ion pair formation and rearrangements and its respective transition states and not on the hydride transfer or the alkoxide transfer transition states.

As for the formation of the first ion pair, 1-Ru-H shows to form a relatively lower ion pair formation in toluene under M06 theory level than $1^{CF2}$-Ru-H; the value of ΔΔG (i.e. the difference between the energies of the similar states at the potential energy diagrams of the two reaction pathways) was found to be +0.6 kcal/mol which indicates a small relative stability of the ion pair of the Milstein catalyst over our proposed catalyst. The values of the bond lengths of C—H in both ion pairs are very similar, with a slight difference in lengths (0.06 Angstroms shorter bond in case of $1^{CF2}$-Ru-H). Similarly, both ion pairs exhibit similar coordination bonds between Ruthenium and the Hydrides, with values of 2.04 and 2.06 Angstroms for 1-Ru-H and $1^{CF2}$-Ru-H respectively, indicating similar activations of the Ruthenium hydride bonds.

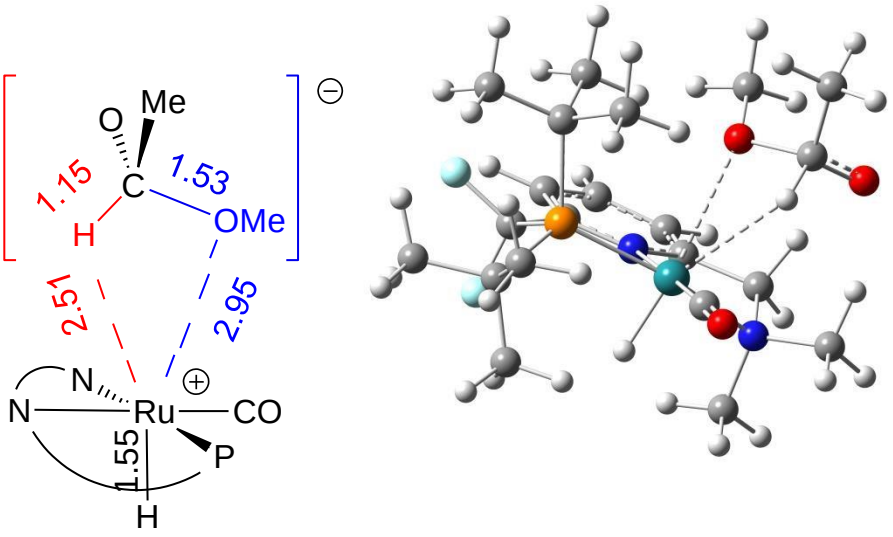


**Figure 3.4:** Slippage transition state for $1^{CF2}$-Ru-H system

The highest points on the potential energy surfaces for both reaction pathways is a slippage transition state in which the C—H and C—OMe bonds on the carbonyl rearrange in a way that the latter would be pointing towards the metal center of the octahedral catalysts. Comparing the transition states of both catalysts, we find out that both show similar values of imaginary frequencies of 106 $cm^{-1}$ and 101.15 $cm^{-1}$ respectively for 1-Ru-H and $1^{CF2}$-Ru-H. The value of ΔΔG was calculated to be +1.8 kcal/mol which indicates that the slippage for the 1-Ru-H is slightly more favorable; this could be due to the fact that we replaced the methylene linker by $CF_2$, since fluorides are more electronegative, they would affect the electronic distribution on the whole catalyst and especially on the Ruthenium atom and its surrounding, which in turn will reduce the negative charge on the hydride so that its transfer would be a bit less favored. Yet, considering the value of ΔΔG (+1.8 kcal/mol) we would infer that the change in electronic properties did not have the drastic effect on the proposed mechanism and the slippage would still be probable for the $1^{CF2}$-Ru-H  The geometries of the slippage transition states for both 1-Ru-H and $1^{CF2}$-Ru-H are quite similar and comparable; with around 0.04 Angstroms difference in Ru—H bonds and Ru—OMe bonds we can still consider both stages to be trending in a similar manner.

The Slippages in both reactions will lead to the formation of the second ion pair in which the Ruthenium will be coordinated to the Methoxy group. Comparing the two ion pairs, we find out that the value of ΔΔG is equal to +3.8 Kcal/mol which is quite significant and in fact being almost double the value of ΔΔG for the slippage (we induce this comparison since we consider the free energy values of the slippage to be the barrier for this reaction). Another parameter to be considered over here is the difference in the calculated bond lengths between the two ion pairs.

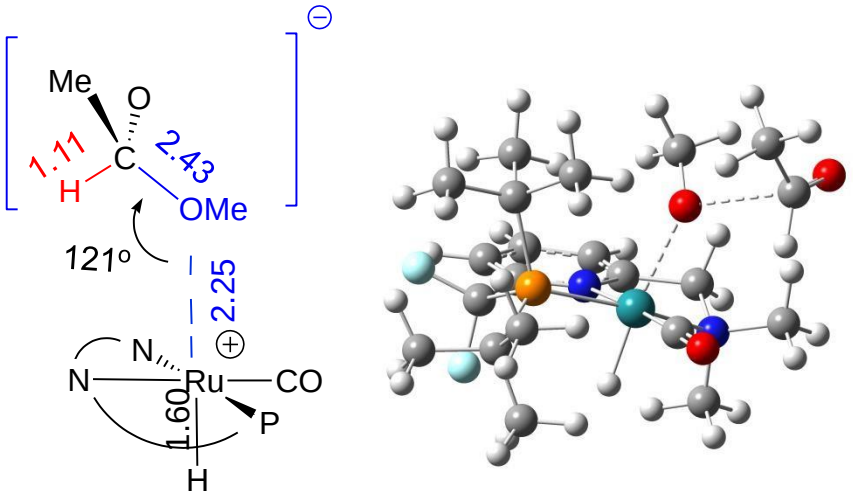


**Figure 3.5:** The aldehyde adduct on the potential energy surface of $1^{CF2}$-Ru-H

In fact, the calculated minimum for the $1^{CF2}$-Ru-H system is not ion pair, unlike the ion pair identified in the previous chapter, this identified complex is an aldehyde adduct. The two ion pairs show a significant difference in the C—O bond lengths, while it was around 1.6 Angstroms in 1-Ru-H, it increased by around 0.83 Angstroms to reach a value of 2.43. Such a value of a C—O bond length is considered to be very high compared to the general values reported for the carbon-oxygen bonds by Allen et al. in their determination of bond lengths by X-ray and neutron diffractions (reported values were in the range of 1.4 Angstroms). This large deviation from the standard values of bond length could be an indicator of the dissociation of the C—O bond and more tendency to form the products. In other words, we can say that the ion pair in $1^{CF2}$-Ru-H would dissociate as soon as it is formed due to first the relatively higher free energy than 1-Ru-H and secondly due to the existence of the long C—O bond. In fact, we can also assume that the calculated minimum does not correspond to an actual ion pair due to the high C—O bond, this effect is due to the smoothness of the potential energy surface, in which the system goes directly into dissociation as soon as it

overcomes the slippage energy barrier, thus the calculated minima is more of a precomplex to the cleavage of the C—OR bond that would eventually lead to the aldehyde and Ru—OMe products. This assumption can be also validated by considering the final products of the reaction.

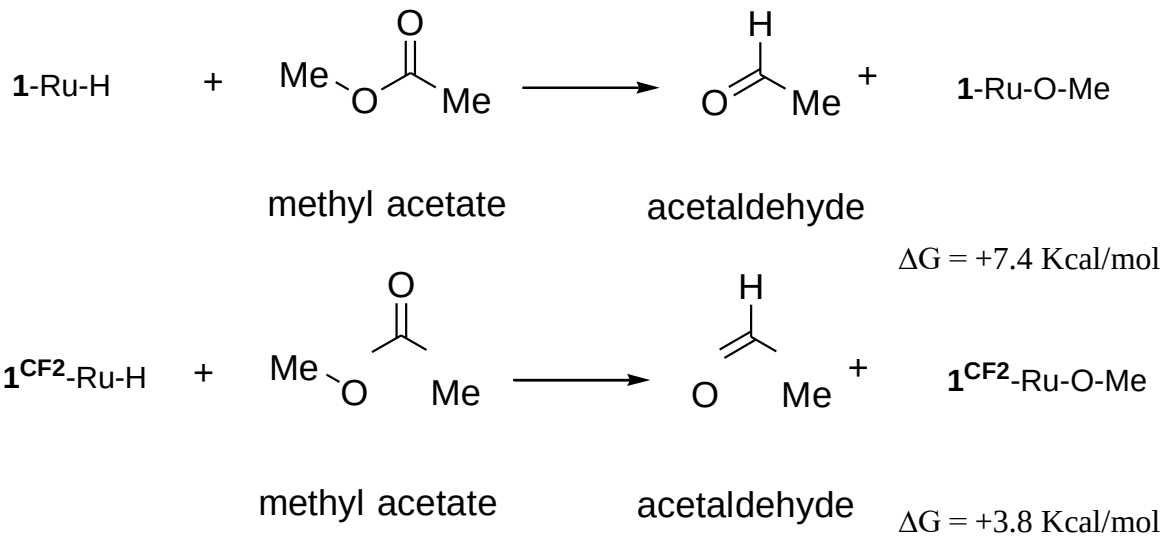


**Figure 3.6:** Thermodynamics of the two metathesis reactions indica[1] products in addition to the values of Gibb's Free Energy for the whole process.

Significantly, the value of ΔG of the second reaction came up to be +3.8 kcal/mol much less than the value of the free energy for the first reaction which was found to be +7.4 kcal/mol. This significant difference in energies (ΔΔG= -3.6 kcal/mol) can be a factor to enhance the efficiency of the $1^{CF2}$-Ru-H potential catalyst as a smaller overall free energy would certainly be thermodynamically more favored. Another factor that could play a role in stabilizing the product of the second reaction over that of the first reaction could be the presence of the two fluorides. As we discussed it previously, the two fluorides affect the partial charge on the Ruthenium atom and thus affect the way that the metal would interact with various electropositive and electronegative atoms. In 1-Ru-OMe, and according to the Mulliken population analysis, the charge on Ru was +0.658 while in $1^{CF2}$-Ru-OMe the charge was found to be +0.750, being more

electropositive; thus our potential catalyst will have more tendency to attract and an increased probability in bonding to the electronegative oxygen of the methoxy group.

### C. Ester Hydrogenation via $1^{O}$-Ru-H

The second potential system we study is the one involving $1^{O}$-Ru-H as the potential catalyst and following the same direct metathesis route as before:

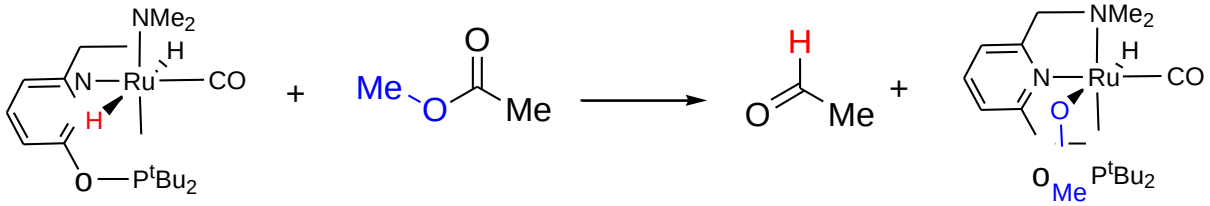


**$1^{O}$-Ru-H** methyl acetate acetaldehyde **$1^{O}$-Ru-O-Me**

The energy comparison between the previously calculated 1-Ru-H system and the potential $1^{O}$-Ru-H system is done under the same level of theory, M06L, and using Toluene as a solvent in SMD continuum. The energy values on different points of the potential energy surface were comparable.

For the initial catalysts, the values of the Ru—H bonds are comparable, with 1.69 and 1.73 Angstroms in the case of $1^{O}$-Ru-H, which is slightly different than the bond lengths in 1-Ru-H (1.71 and 1.73 Angstroms). This indicates, in a similar manner for $1^{CF2}$-Ru-H, that the trans hydrides are not equivalent and eventually one is more activated and can be transferred to the substrate. In addition, the puckered geometry of the two catalysts would be another factor that enhances the exposing of the hydride to the carbonyl and provide the suitable space for the substrate to fit into the catalyst.

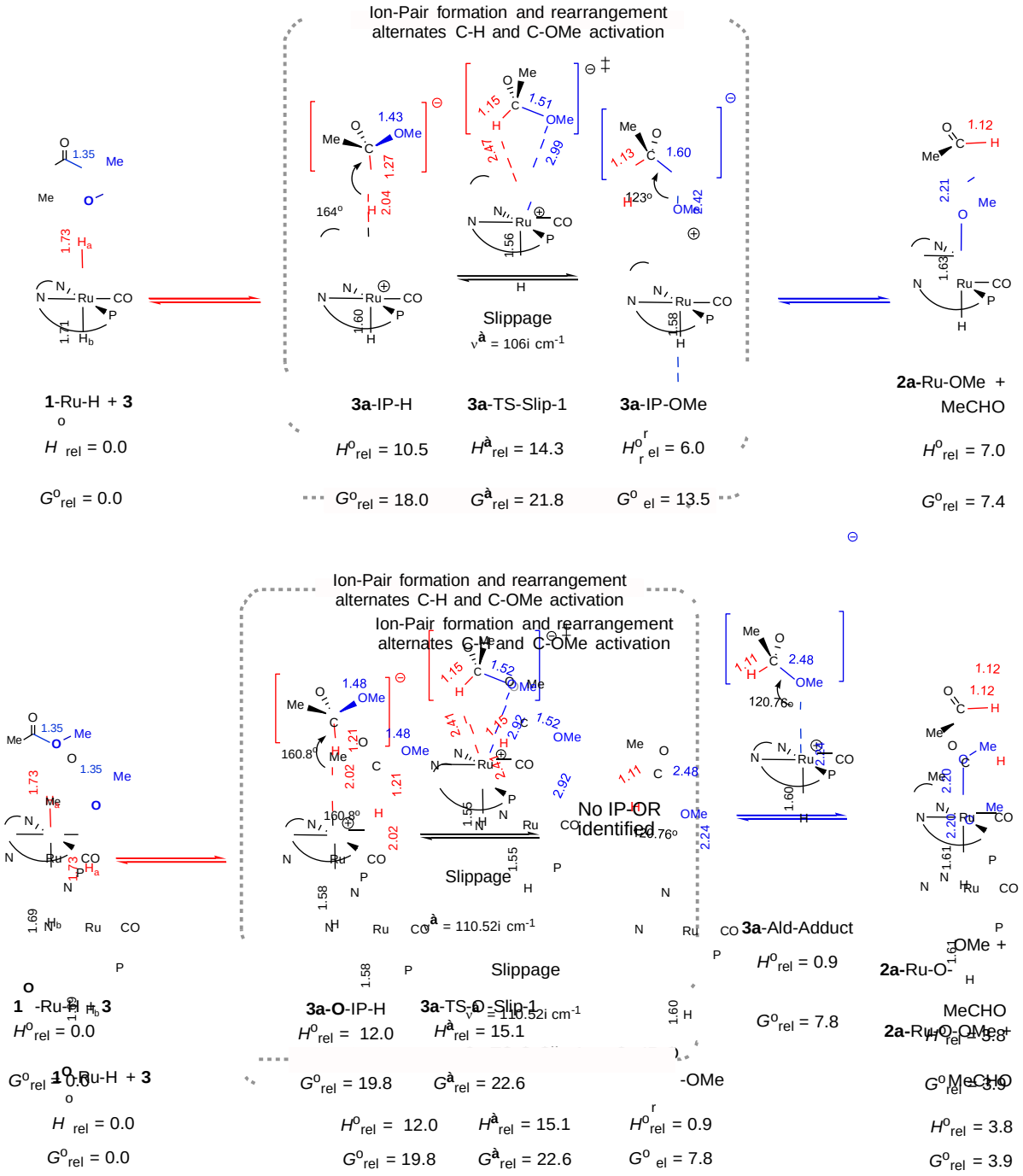


**Figure 3.7:** Comparison of the potential energy surface of the catalysis using 1-Ru-H (top) and $1^{O}$-Ru-H (bottom) under M06 level using toluene as a solvent.

As for the formation of the first ion pair, 1-Ru-H shows to form a relatively lower ion pair formation in toluene under M06 theory level than $1^{O}$-Ru-H; the value of ΔΔG (i.e. the difference between the energies of the similar states at the potential energy diagrams of the two reaction pathways) was found to be +1.8 kcal/mol

which indicates a small relative stability of the ion pair of the Milstein catalyst over our potential catalyst. The values of the bond lengths of C—H in both ion pairs are very similar, 3a-IP-H has a C—H value of 1.27 Angstrom while 3a-O-IP-H shows a value of 1.21 Angstroms, with a slight difference in lengths (0.06 Angstroms shorter bond in case of $1^{O}$-Ru-H). Also, both ion pairs exhibit similar coordination bonds between

Ruthenium and the Hydrides, with values of 2.04 and 2.02 Angstroms for 1-Ru-H and $1^{O}$-Ru-H respectively, indicating that the activation of the Ru—H bonds are occurring in a very similar manner.

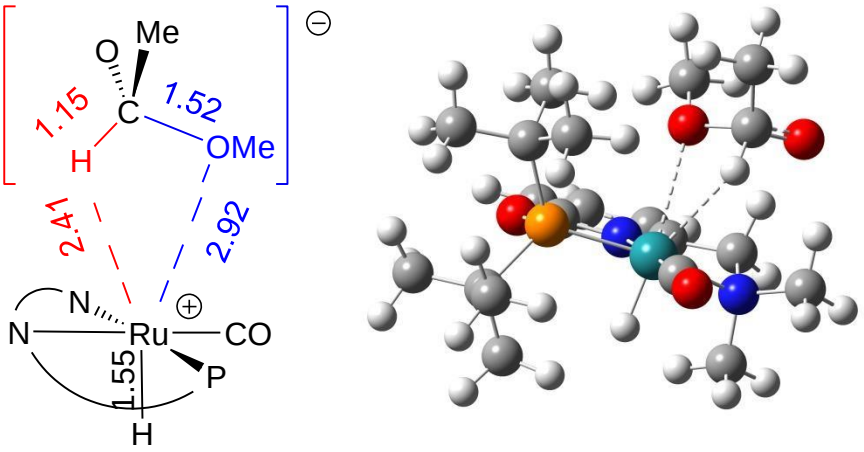


**Figure 3.8:** Slippage transition state for $1^{O}$-Ru-H system

Next we take a look at the transition state of the chemical reaction. The slippage transition state occurs similarly here where the C—H and C—OMe bonds on the carbonyl rearrange in a way that the latter would be pointing towards the Ruthenium metal center of the octahedral catalysts. Comparing the transition states of both catalysts, we find out that both show similar values of imaginary frequencies of 106 $cm^{-1}$ and 110.52 $cm^{-1}$ respectively for 1-Ru-H and $1^{O}$-Ru-H. The value of ΔΔG was calculated to be +0.8 kcal/mol, 1 kcal/mol less than the difference between slippages of 1-Ru-H and $1^{CF2}$-Ru-H. Also, the geometries of the slippage transition states for both 1-Ru-H and $1^{O}$-Ru-H are quite similar and comparable; the Ru—H bond in $1^{O}$-Ru-H system is 2.41, being 0.06 Angstroms shorter than the slippage in 1-Ru-H, similar values of Ru—O bond lengths are obtained, with 2.92 for $1^{O}$-Ru-H compared to the very slightly longer value (2.99 Angstroms) for 1-Ru-H.

The Slippages in both reactions will lead to the formation of the second ion pair in which the Ruthenium will be coordinated to the Methoxy group. Comparing the two ion pairs, we find out that the value of ΔΔG is equal to -5.7 Kcal/mol which is quite considerable. Unlike the $1^{CF2}$-Ru-H system, in $1^{O}$-Ru-H; calculated minimum shows a significant stability relative to the corresponding slippage transition state. Another parameter to be considered over here is the difference in the calculated bond lengths between the two ion pairs.

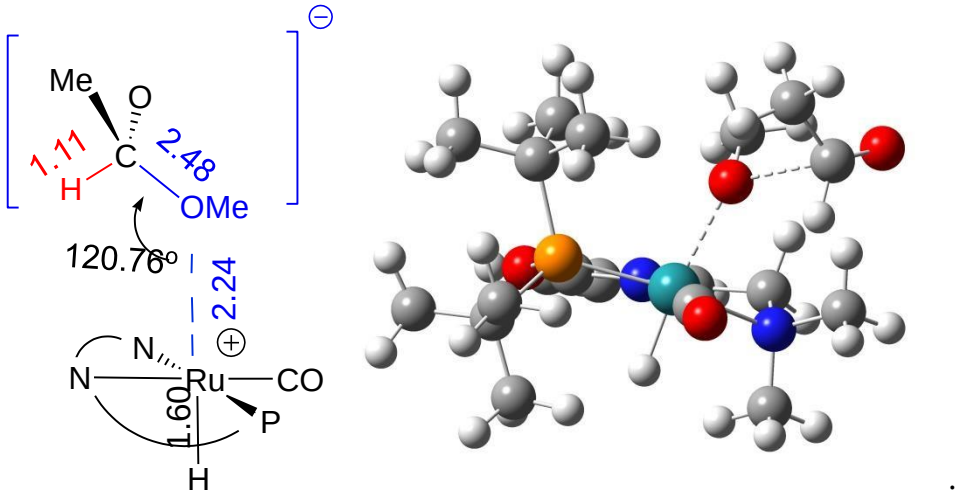


**Figure 3.9:** The aldehyde adduct on the potential energy surface of $1^{O}$-Ru-H

The two ion pairs show a significant difference in the C—O bond lengths, while it was around 1.6 Angstroms in 1-Ru-H, it increased by around 0.88 Angstroms to reach a value of 2.48. Also in this case, the bond length of C—O is considered to be very high compared to the general values reported for the carbon-oxygen bonds by Allen et al. in their determination of bond lengths by X-ray and neutron diffractions (reported values were in the range of 1.4 Angstroms). This large deviation from the standard values of bond length could be an indicator of the dissociation of the C—O

bond and more tendency to form the products. In other words, we can say that the second ion pair in $1^{O}$-Ru-H, same as in the case of $1^{CF2}$-Ru-H, would dissociate as soon as it is formed due to first the relatively higher free energy than that of 1-Ru-H and secondly due to the existence of the long C—O bond. In fact, we can also assume that the calculated minimum does not correspond to an actual ion pair due to the high C—O bond, this effect is due to the smoothness of the potential energy surface, in which the system goes directly into dissociation as soon as it overcomes the slippage energy barrier. Similar to the $1^{CF2}$-Ru-H case, the calculated minimum on the PES corresponds to an aldehyde adduct that is a precomplex to the dissociation of the C—OR bond cleavage.

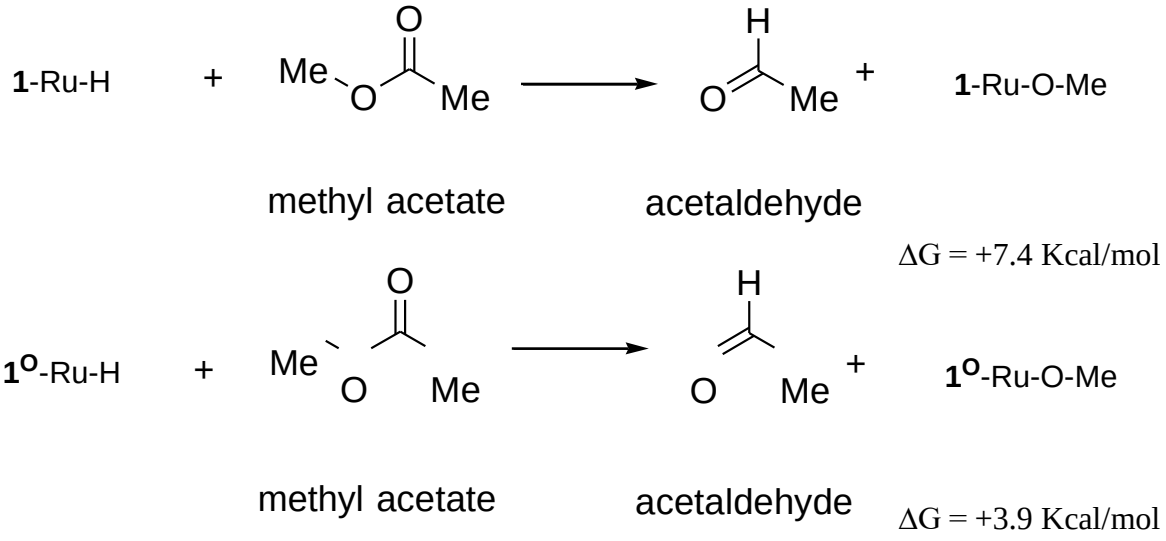


**Figure 3.10:** Thermodynamics of the two metathesis reactions indicating initial and final products in addition to the values of Gibb's Free Energy for the whole pathway.

Significantly, the value of ΔG of the second reaction came up to be +3.9 kcal/mol, which is much less than the value of the free energy for the first reaction which was found to be +7.4 kcal/mol. This significant difference in energies, same as the case of the previous potential system, which is found to be ΔΔG= -3.5 kcal/mol,

can be a factor to enhance the efficiency of the $1^{O}$-Ru-H potential catalyst as a smaller overall free energy would certainly be thermodynamically more favored.

## D. Conclusion

Upon building up potential catalyst systems by replacing the methylinic linker by one that lacks the acidic protons that are the highlight of the generally accepted Metal-Ligand Cooperation, we were still able to identify similar potential energy surfaces to our proposed mechanism. This would imply that the presence of the methylinic protons is insignificant in the hydrogenation of esters.

# CHAPTER IV

# CONCLUSION

In conclusion, we present in this study and using electronic structure DFT methods, an alternative metathesis mechanism to the dehydrogenative coupling of alcohols and amides into esters and carboxamides. The identified route is a more direct, low energy route to the coupling that involves formation of two ion pairs mediated by a simple rearrangement within the ion-pairs to transfer the hydride from the metal center to the substrate. Two key features of the proposed mechanism include a direct metathesis route and a lower potential energy system compared to the generally accepted Metal-Ligand Cooperation mechanism.

In addition, DFT calculations on potential systems showed that the absence of the methylinic proton, which plays an essential role in MLC mechanism, would not have an effect on the calculated energies for the slippage mechanisms of systems involving two different potential catalysts for ester hydrogenation.

The study paves the way to reconsidering the Metal-Ligand Cooperation mechanism that has been thought of to be as a generally accepted mechanism and to start pointing out more direct metathesis mechanisms that do not involve the modification of the ligand or part of it. Moreover, Milstein and co. are still in the process of synthesizing new catalysts and reporting  new transformations, so theoretical studies will still be necessary to explain the mechanisms of these systems. Considering a newly proposed mechanism could be helpful in directing the mechanistic studies into more vivid conclusions.

# REFERENCES


1. *What is Green Chemistry?* [cited 2015 March 31]; Available from: https://www.acs.org/content/acs/en/greenchemistry/what-is-green-chemistry.html.

2. Anastas, P. and N. Eghbali, *Green chemistry: principles and practice.* Chemical Society Reviews. **39**(1): p. 301-312.

3. Milstein, D., *Discovery of environmentally benign catalytic reactions of alcohols catalyzed by pyridine-based pincer Ru complexes, based on metal-ligand cooperation.* Topics in Catalysis. **53**(13-14): p. 915-923.

4. Carey, F.A. and R.J. Sundberg, *Advanced Organic Chemistry: Part A: Structure and Mechanisms*. 2007: Springer Science & Business Media.

5. [cited 2015 April]; Available from: http://www.inchem.org/documents/icsc/icsc/eics0913.htm.

6. Finholt, A., A. Bond Jr, and H. Schlesinger, *Lithium aluminum hydride, aluminum hydride and lithium gallium hydride, and some of their applications in organic and inorganic Chemistry1*. Journal of the American Chemical Society, 1947. **69**(5): p. 1199-1203.

7. Clarke, M.L., *Recent developments in the homogeneous hydrogenation of carboxylic acid esters.* Catalysis Science & Technology. **2**(12): p. 2418-2423.

8. Gunanathan, C. and D. Milstein, *Metal-Ligand Cooperation by Aromatization-Dearomatization: A New Paradigm in Bond Activation and â€œGreenâ€• Catalysis.* Accounts of chemical research. **44**(8): p. 588-602.

9. Li, H. and M.B. Hall, *Computational Mechanistic Studies on Reactions of Transition Metal Complexes with Noninnocent Pincer Ligands: Aromatization-Dearomatization or Not.* ACS Catalysis. **5**(3): p. 1895-1913.

10. Atkins, R.C. and F.A. Carey, *Organic chemistry: a brief course*. 2002: McGraw-Hill.

11. Zhang, J., et al., *Electron-rich PNP-and PNN-type ruthenium (II) hydrido borohydride pincer complexes. Synthesis, structure, and catalytic dehydrogenation of alcohols and hydrogenation of esters.* Organometallics. **30**(21): p. 5716-5724.

12. Zhang, J., et al., *Facile conversion of alcohols into esters and dihydrogen catalyzed by new ruthenium complexes.* Journal of the American Chemical Society, 2005. **127**(31): p. 10840-10841.

13. Balaraman, E., Y. Ben•David, and D. Milstein, *Unprecedented catalytic hydrogenation of urea derivatives to amines and methanol.* Angewandte Chemie. **123**(49): p. 11906-11909.

14. Balaraman, E., et al., *Efficient hydrogenation of organic carbonates, carbamates and formates indicates alternative routes to methanol based on CO2 and CO.* Nature chemistry. **3**(8): p. 609-614.

15. Gunanathan, C. and D. Milstein, *Applications of acceptorless dehydrogenation and related transformations in chemical synthesis.* Science. **341**(6143): p. 1229712.

16. Morales-Morales, D. and C.G. Jensen, *The chemistry of pincer compounds*: Elsevier.

17. Wanniarachchi, S., et al., *Preparation, properties, and reactivity of carbonylrhodium (I) complexes of di (2-pyrazolylaryl) amido-pincer ligands.* Journal of Organometallic Chemistry. **696**(23): p. 3623-3636.

18. Schuster, E.M., M. Botoshansky, and M. Gandelman, *Pincer click ligands.* Angewandte Chemie International Edition, 2008. **47**(24): p. 4555-4558.

19. Van der Boom, M.E. and D. Milstein, *Cyclometalated phosphine-based pincer complexes: mechanistic insight in catalysis, coordination, and bond activation.* Chemical reviews, 2003. **103**(5): p. 1759-1792.

20. Lee, H.M., et al., *A new tridentate pincer phosphine/N-heterocyclic carbene ligand: Palladium complexes, their structures, and catalytic activities.* Inorganic chemistry, 2004. **43**(21): p. 6822-6829.

21. Roddick, D.M., *Tuning of PCP pincer ligand electronic and steric properties*, in *Organometallic Pincer Chemistry*, Springer. p. 49-88.

22. Dani, P., et al., *Hydrogen•transfer catalysis with pincer-aryl ruthenium (ii) Complexes.* Angewandte Chemie International Edition, 2000. **39**(4): p. 743-745.

23. Collman, J., et al., *Principles and applications of organometallic chemistry.* Principles and Applications of Organometallic Chemistry, 1987.

24. Zhang, J., et al., *Iron (II) complexes based on electron-rich, bulky PNN-and PNP-type ligands.* Inorganica chimica acta, 2006. **359**(6): p. 1955-1960.

25. Gnanaprakasam, B., Y. Ben•David, and D. Milstein, *Ruthenium Pincer Catalyzed Acylation of Alcohols Using Esters with Liberation of Hydrogen under Neutral Conditions.* Advanced Synthesis & Catalysis. **352**(18): p. 3169-3173.

26. Srimani, D., et al., *Ruthenium Pincer Catalyzed Cross Dehydrogenative Coupling of Primary Alcohols with Secondary Alcohols under Neutral Conditions.* Advanced Synthesis & Catalysis. **354**(13): p. 2403-2406.

27. Zhang, J., et al., *Efficient homogeneous catalytic hydrogenation of esters to alcohols.* Angewandte Chemie International Edition, 2006. **45**(7): p. 1113-1115.

28. Balaraman, E., et al., *Direct hydrogenation of amides to alcohols and amines under mild conditions.* Journal of the American Chemical Society. **132**(47): p. 16756-16758.

29. Noyori, R., *Asymmetric catalysis: science and opportunities (Nobel lecture).* Angewandte Chemie International Edition, 2002. **41**(12): p. 2008-2022.

30. Noyori, R. and S. Hashiguchi, *Asymmetric transfer hydrogenation catalyzed by chiral ruthenium complexes.* Accounts of chemical research, 1997. **30**(2): p. 97-102.

31. Gunanathan, C. and D. Milstein, *Bond activation by metal-ligand cooperation: Design of green catalytic reactions based on aromatization-dearomatization of pincer complexes*, in *Bifunctional Molecular Catalysis*, Springer. p. 55-84.

32. Iron, M.A., et al., *Metal-ligand cooperation in the trans addition of dihydrogen to a pincer Ir (I) complex: a DFT study.* Dalton Transactions, 2009(43): p. 9433-9439.

33. Schwartsburd, L., et al., *Synthesis and Reactivity of an Iridium (I) Acetonyl PNP Complex. Experimental and Computational Study of Metal Ligand Cooperation in H–H and C–H Bond Activation via Reversible Ligand Dearomatization.* Organometallics. **29**(17): p. 3817-3827.

34. Wiberg, K.B., K.M. Morgan, and H. Maltz, *Thermochemistry of carbonyl reactions. 6. A study of hydration equilibria.* Journal of the American Chemical Society, 1994. **116**(24): p. 11067-11077.

35. Balcells, D., et al., *Mechanism of homogeneous iridium-catalyzed alkylation of amines with alcohols from a DFT study.* Organometallics, 2008. **27**(11): p. 2529-2535.

36. Hamid, M.H.S. and J.M. Williams, *Ruthenium catalysed N-alkylation of amines with alcohols.* Chemical communications, 2007(7): p. 725-727.

37. Nova, A., et al., *An Experimental Theoretical Study of the Factors That Affect the Switch between Ruthenium-Catalyzed Dehydrogenative Amide Formation versus Amine Alkylation.* Organometallics. **29**(23): p. 6548-6558.

38. Gnanaprakasam, B., J. Zhang, and D. Milstein, *Direct synthesis of imines from alcohols and amines with liberation of H2.* Angewandte Chemie International Edition. **49**(8): p. 1468-1471.

39. Li, H., et al., *Computational study on the catalytic role of pincer ruthenium (II)-PNN complex in directly synthesizing amide from alcohol and amine: The origin of selectivity of amide over ester and imine.* Organometallics. **30**(19): p. 5233-5247.

40. Cho, D., K.C. Ko, and J.Y. Lee, *Catalytic mechanism for the ruthenium-complex-catalyzed synthesis of amides from alcohols and amines: a DFT study.* Organometallics. **32**(16): p. 4571-4576.

41. Li, H., M. Wen, and Z.-X. Wang, *Computational Mechanistic Study of the Hydrogenation of Carbonate to Methanol Catalyzed by the Ru-II PNN Complex.* Inorganic chemistry. **51**(10): p. 5716-5727.

42. Frisch, M.J., et al., *Gaussian 09*. 2009, Gaussian, Inc.: Wallingford, CT, USA.

43. Zhao, Y. and D.G. Truhlar, *The M06 suite of density functionals for main group thermochemistry, thermochemical kinetics, noncovalent interactions, excited states, and transition elements: two new functionals and systematic testing of four M06-class functionals and 12 other functionals.* Theoretical Chemistry Accounts, 2008. **120**(1-3): p. 215-241.

44. McLean, A. and G. Chandler, *Contracted Gaussian basis sets for molecular calculations. I. Second row atoms, Z= 11-18.* The Journal of Chemical Physics, 1980. **72**(10): p. 5639-5648.

45. Rassolov, V.A., et al., *6-31G* basis set for third•row atoms.* Journal of Computational Chemistry, 2001. **22**(9): p. 976-984.

46. Hollwarth, A., et al., *A set of d-polarization functions for pseudo-potential basis sets of the main group elements Alî—¸ Bi and f-type polarization functions for Zn, Cd, Hg.* Chemical physics letters, 1993. **208**(3): p. 237-240.

47. Fukui, K., *The path of chemical reactions-the IRC approach.* Accounts of chemical research, 1981. **14**(12): p. 363-368.

48. Zhao, Y. and D.G. Truhlar, *A new local density functional for main-group thermochemistry, transition metal bonding, thermochemical kinetics, and noncovalent interactions.* The Journal of Chemical Physics, 2006. **125**(19): p. 194101.

49. Chai, J.-D. and M. Head-Gordon, *Long-range corrected hybrid density functionals with damped atom-atom dispersion corrections.* Physical Chemistry Chemical Physics, 2008. **10**(44): p. 6615-6620.

50. Marenich, A.V., C.J. Cramer, and D.G. Truhlar, *Universal solvation model based on solute electron density and on a continuum model of the solvent defined by the bulk dielectric constant and atomic surface tensions.* The Journal of Physical Chemistry B, 2009. **113**(18): p. 6378-6396.

51. Averkiev, B.B. and D.G. Truhlar, *Free energy of reaction by density functional theory: oxidative addition of ammonia by an iridium complex with PCP pincer ligands.* Catalysis Science & Technology. **1**(8): p. 1526-1529.

52. Gusev, D.G., *Assessing the Accuracy of M06-L Organometallic Thermochemistry.* Organometallics. **32**(15): p. 4239-4243.

53. Pudasaini, B. and B.G. Janesko, *Agostic interactions in nickel (II) complexes: trans influence of ancillary ligands on the strength of the bond.* Organometallics. **33**(1): p. 84-93.

54. Remya, K. and C.H. Suresh, *Which density functional is close to CCSD accuracy to describe geometry and interaction energy of small noncovalent dimers? A benchmark study using Gaussian09.* Journal of Computational Chemistry. **34**(15): p. 1341-1353.

55. Hasanayn, F. and A. Baroudi, *Direct H/OR and OR/ORâ€² Metathesis Pathways in Ester Hydrogenation and Transesterification by Milstein's Catalyst.* Organometallics. **32**(9): p. 2493-2496.

56. Hasanayn, F., et al., *Hydrogenation of Dimethyl Carbonate to Methanol by trans-[Ru (H) 2 (PNN)(CO)] Catalysts: DFT Evidence for Ion-Pair-Mediated Metathesis Paths for Câ€“OMe Bond Cleavage.* Organometallics. **32**(23): p. 6969-6985.

57. Yang, X., *Unexpected Direct Reduction Mechanism for Hydrogenation of Ketones Catalyzed by Iron PNP Pincer Complexes.* Inorganic chemistry. **50**(24): p. 12836-12843.

58. Casey, C.P., et al., *Hydrogen elimination from a hydroxycyclopentadienyl ruthenium (II) hydride: Study of hydrogen activation in a ligand-metal bifunctional hydrogenation catalyst.* Journal of the American Chemical Society, 2005. **127**(9): p. 3100-3109.

59. Zhang, X., et al., *Mechanism investigation of ketone hydrogenation catalyzed by ruthenium bifunctional catalysts: insights from a DFT study.* Physical Chemistry Chemical Physics. **14**(17): p. 6003-6012.

60. Sandoval, C.A., et al., *Mechanism of asymmetric hydrogenation of ketones catalyzed by BINAP/1, 2-diamine-ruthenium (II) complexes.* Journal of the American Chemical Society, 2003. **125**(44): p. 13490-13503.

61. Hedberg, C., et al., *Mechanistic insights into the phosphine-free RuCp*-diamine-catalyzed hydrogenation of aryl ketones: Experimental and theoretical evidence for an alcohol-mediated dihydrogen activation.* Journal of the American Chemical Society, 2005. **127**(43): p. 15083-15090.

62. Findlater, M., W.H. Bernskoetter, and M. Brookhart, *Proton-Catalyzed Hydrogenation of a d8 Ir (I) Complex Yields a trans Ir (III) Dihydride.* Journal of the American Chemical Society. **132**(13): p. 4534-4535.

63. Dub, P.A. and T. Ikariya, *Catalytic reductive transformations of carboxylic and carbonic acid derivatives using molecular hydrogen.* ACS Catalysis. **2**(8): p. 1718-1741.

64. Takebayashi, S. and S.H. Bergens, *Facile bifunctional addition of lactones and esters at low temperatures. the first intermediates in lactone/ester hydrogenations.* Organometallics, 2009. **28**(8): p. 2349-2351.

65. Baratta, W., et al., *Ruthenium (II) Terdentate CNN Complexes: Superlative Catalysts for the Hydrogen•Transfer Reduction of Ketones by Reversible Insertion of a Carbonyl Group into the Ruï£¿ H Bond.* Angewandte Chemie International Edition, 2005. **44**(38): p. 6214-6219.

66. Baratta, W., et al., *Terdentate RuX (CNN)(PP)(X= Cl, H, OR) complexes: synthesis, properties, and catalytic activity in fast transfer hydrogenation.* Organometallics, 2006. **25**(19): p. 4611-4620.

67. Zhang, Y., et al., *Innate immune responses of synthetic lipid A derivatives of Neisseria meningitidis.* Chemistry-A European Journal, 2008. **14**(2): p. 558-569.

68. Hamilton, R.J., et al., *A ruthenium-dihydrogen putative intermediate in ketone hydrogenation.* Journal of the American Chemical Society, 2005. **127**(12): p. 4152-4153.

69. Hamilton, R.J. and S.H. Bergens, *An unexpected possible role of base in asymmetric catalytic hydrogenations of ketones. Synthesis and characterization of several key catalytic intermediates.* Journal of the American Chemical Society, 2006. **128**(42): p. 13700-13701.

70. Hamilton, R.J. and S.H. Bergens, *Direct Observations of the Metal- Ligand Bifunctional Addition Step in an Enantioselective Ketone Hydrogenation.* Journal of the American Chemical Society, 2008. **130**(36): p. 11979-11987.

71. Takebayashi, S., et al., *Experimental Investigations of a Partial Ru-O Bond during the Metal-Ligand Bifunctional Addition in Noyori-Type Enantioselective Ketone Hydrogenation.* Journal of the American Chemical Society. **133**(25): p. 9666-9669.

72. Bertoli, M., et al., *Osmium and ruthenium catalysts for dehydrogenation of alcohols.* Organometallics. **30**(13): p. 3479-3482.

73. Spasyuk, D. and D.G. Gusev, *Acceptorless dehydrogenative coupling of ethanol and hydrogenation of esters and imines.* Organometallics. **31**(15): p. 5239-5242.

74. Darensbourg, D.J., et al., *Kinetic and Thermodynamic Investigations of CO2 Insertion Reactions into Ru-Me and Ru-H Bonds "An Experimental and Computational Study.* European Journal of Inorganic Chemistry. **2013**(22-23): p. 4024-4031.

75. Darensbourg, D.J., A. Rokicki, and M.Y. Darensbourg, *Facile reduction of carbon dioxide by anionic Group 6b metal hydrides. Chemistry relevant to catalysis of the water-gas shift reaction.* Journal of the American Chemical Society, 1981. **103**(11): p. 3223-3224.

76. Darensbourg, D.J., et al., *A kinetic investigation of carbon dioxide insertion processes involving anionic tungsten-alkyl and-aryl derivatives: effects of carbon dioxide pressure, counterions, and ancillary ligands. Comparisons with migratory carbon monoxide insertion processes.* Journal of the American Chemical Society, 1985. **107**(25): p. 7463-7473.

77. Langer, R., et al., *Low•Pressure Hydrogenation of Carbon Dioxide Catalyzed by an Iron Pincer Complex Exhibiting Noble Metal Activity.* Angewandte Chemie International Edition. **50**(42): p. 9948-9952.

78. Salem, H., et al., *Formation of Stable trans-Dihydride Ruthenium (II) and 16-Electron Ruthenium (0) Complexes Based on Phosphinite PONOP Pincer Ligands. Reactivity toward Water and Electrophiles.* Organometallics, 2009. **28**(16): p. 4791-4806.

79. Schmeier, T.J., et al., *Secondary coordination sphere interactions facilitate the insertion step in an iridium (III) CO2 reduction catalyst.* Journal of the American Chemical Society. **133**(24): p. 9274-9277.

80. Whittlesey, M.K., R.N. Perutz, and M.H. Moore, *Facile Insertion of CO2 into the Ru-H Bonds of Ru (dmpe) 2H2 (dmpe= Me2PCH2CH2PMe2): Identification of Three Ruthenium Formate Complexes.* Organometallics, 1996. **15**(24): p. 5166-5169.

81. Blum, O. and D. Milstein, *Hydride elimination from an iridium (III) alkoxide complex: a case in which a vacant cis coordination site is not required.* Journal of Organometallic Chemistry, 2000. **593**: p. 479-484.

82. Fafard, C.M. and O.V. Ozerov, *Retardation of Î²-hydrogen elimination in PNP Pincer complexes of Pd.* Inorganica chimica acta, 2007. **360**(1): p. 286-292.

83. Smythe, N.A., et al., *Reductive Elimination and Dissociative Î²-Hydride Abstraction from Pt (IV) Hydroxide and Methoxide Complexes.* Organometallics, 2008. **28**(1): p. 277-288.

84. Hasanayn, F. and R.H. Morris, *Symmetry Aspects of H2 Splitting by Five-Coordinate d6 Ruthenium Amides, and Calculations on Acetophenone Hydrogenation, Ruthenium Alkoxide Formation, and Subsequent Hydrogenolysis in a Model trans-Ru (H) 2 (diamine)(diphosphine) System.* Inorganic chemistry. **51**(20): p. 10808-10818.

85. Handgraaf, J.-W. and E.J. Meijer, *Realistic modeling of ruthenium-catalyzed transfer hydrogenation.* Journal of the American Chemical Society, 2007. **129**(11): p. 3099-3103.